

Spontaneous condensation of saturated vapour in a corner formed by two walls

E. S. Benilov[†]

Department of Mathematics and Statistics, University of Limerick,
Limerick V94 T9PX, Ireland

(Received xx; revised xx; accepted xx)

This paper examines the dynamics of saturated vapour in a corner formed by two walls. It is shown that, if the angle ϕ between the walls is sufficiently small, the vapor becomes unstable and spontaneous condensation occurs near the corner, giving rise to an ever-growing liquid meniscus. The diffuse-interface model and the lubrication approximation are used to demonstrate that the condensation occurs if and only if $\phi + 2\theta < \pi$, where θ is the contact angle corresponding to the fluid–solid combination under consideration. This criterion has a simple physical explanation: if it holds, the meniscus surface is concave – hence, the so-called Kelvin effect causes condensation. If the near-vertex region of the corner is smoothed, the instability can be triggered off only by a *finite*-size perturbation, with enough liquid to cover the smoothed area by a microscopically-thin liquid film.

1. Introduction

Saturated vapour and liquid are supposed to be in thermodynamic equilibrium – thus, if a small amount of the latter is placed in a container filled with the former, no exchange of mass should occur.

This simple conclusion – no matter how natural – is misleading: if the liquid is placed in a sufficiently acute (or not too obtuse) corner, mass exchange does occur. This result is obtained in the present paper for a narrow range of parameters, using an elaborate mathematical model – but it agrees with the fundamental properties of interfaces and, therefore, is likely to hold generally.

Consider a small meniscus in a corner formed by two walls intersecting at an angle ϕ (see figure 1), and assume, for the time being, that the meniscus is static. Introduce also the contact angle θ at which the meniscus free boundary approaches the walls. Theoretically, θ is specific to the fluid–substrate combination under consideration, but in reality the walls are never perfectly flat and chemically homogeneous. Microscopic imperfections give rise to a hysteresis interval, i.e., a certain spread in θ ; in what follows, it is assumed narrow – hence, insignificant – and is neglected.

Now, let ϕ and θ be such that

$$\phi + 2\theta < \pi, \quad (1.1)$$

in which case the free surface of the meniscus is concave (see figure 1). As a result, the so-called Kelvin effect (Eggers & Pismen 2010; Colinet & Rednikov 2011; Rednikov & Colinet 2013; Morris 2014; Janeček *et al.* 2015; Saxton *et al.* 2016; Rednikov & Colinet 2017, 2019) gives rise to a vapour-to-liquid mass flux, making the meniscus absorb fluid from the surrounding vapour and grow – which can be viewed as an instability of the vapour near the corner. Even if the flow dynamics alters the static contact angle, it

[†] Email address for correspondence: Eugene.Benilov@ul.ie

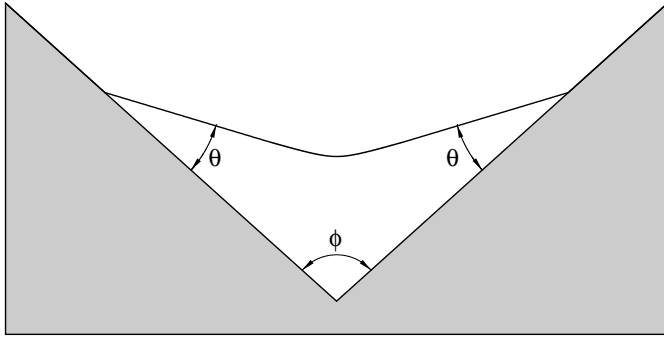


Figure 1: A liquid meniscus in a corner between two solids. In the configuration shown, the contact angle θ is such that $\phi + 2\theta < \pi$, so spontaneous condensation occurs.

cannot stop the expansion of the meniscus: if it could, θ would regain its static value satisfying condition (1.1) and the expansion would resume.

If, on the other hand, condition (1.1) does *not* hold, the surface of the meniscus is convex, and the Kelvin effect makes it dry up. This explains physically the nonexistence of solutions describing static liquid ridges (Benilov 2020*d*) and three-dimensional drops (Benilov 2021) – in both cases, on a flat substrate and surrounded by saturated vapour.

Neither of the two possible behaviours of menisci can be described by the classical Navier–Stokes equations, which miss both condensation and evaporation; instead, these effects are typically accounted for by coupling the liquid dynamics to vapour diffusion in the surrounding air (e.g. Deegan *et al.* 2000; Eggers & Pismen 2010; Colinet & Rednikov 2011; Rednikov & Colinet 2013; Morris 2014; Janeček *et al.* 2015; Stauber *et al.* 2015; Saxton *et al.* 2016; Brabcova *et al.* 2017; Rednikov & Colinet 2019; Wray *et al.* 2019). Alternatively (as done in the present paper), the problem can be examined using the diffuse-interface model: it includes both hydro- and thermodynamics and, thus, consistently describes all of the effects arising in the problem at hand.

The diffuse-interface model (DIM) was invented as a tool for modeling interfaces; it is based on two assumptions put forward by Korteweg (1901), and later developed by Ginzburg (1960) and Cahn (1961):

(i) the van der Waals intermolecular force (responsible for phase transitions) can be described by a pair-wise potential,

(ii) the characteristic length of this potential is much smaller than the interfacial thickness.

In recent times, the DIM has been used in numerous problems including nucleation and collapse of bubbles (Magaletti *et al.* 2015, 2016; Gallo *et al.* 2018, 2020), phase separation in polymer blends (Thiele *et al.* 2007; Madruga & Thiele 2009), contact lines in liquid (Ding & Spelt 2007; Yue *et al.* 2010; Yue & Feng 2011; Sibley *et al.* 2013*a,b*, 2014; Borcica & Bestehorn 2014; Borcica *et al.* 2019), *etc.*

The present paper employs the DIM version of Anderson *et al.* (1998); Pismen & Pomeau (2000), under an additional assumption that the angle between the intersecting walls is almost straight ($\phi \approx \pi$) and they are made of a hydrophilic material ($\theta \ll 1$). This way, one can simplify the problem through the lubrication approximation (applicable to menisci with a small slope of the free surface) – and even more so, since the lubrication approximation for a flat substrate ($\phi = \pi$) is already in place (Benilov 2020*c*).

In §2 of the present paper, the problem will be formulated mathematically. §§3–4 examine solutions describing static and evolving menisci, respectively. §5 explains why the effect of spontaneous condensation has yet to be observed experimentally (in a nutshell, because growing menisci take several hours to several days to reach a macroscopic scale). The lubrication approximation of the DIM is derived in Appendix B and summarised in §6 in a form that can be used for modeling thin sessile drops with moving contact lines.

2. Formulation

2.1. Thermodynamics

The thermodynamic properties of a fluid can be described by the dependence of its internal energy e and entropy s (both specific, or per unit mass) on the density ρ and temperature T . The functions $e(\rho, t)$ and $s(\rho, t)$ are not fully arbitrary, as they should satisfy the fundamental thermodynamic relation amounting to

$$\frac{\partial e}{\partial T} = T \frac{\partial s}{\partial T}. \quad (2.1)$$

Then, the equation of state (the expression for the pressure p) is given by

$$p = \rho^2 \left(\frac{\partial e}{\partial \rho} - T \frac{\partial s}{\partial \rho} \right), \quad (2.2)$$

and the specific chemical potential (Gibbs free energy), by

$$G = e - Ts + \frac{p}{\rho}. \quad (2.3)$$

It follows from (2.1)–(2.3) that

$$\frac{\partial p}{\partial \rho} = \rho \frac{\partial G}{\partial \rho}, \quad \frac{\partial p}{\partial T} = \rho \left(\frac{\partial G}{\partial T} + s \right), \quad (2.4)$$

$$G = \frac{\partial}{\partial \rho} (\rho G - p), \quad (2.5)$$

$$\frac{\partial G}{\partial T} = - \frac{\partial (\rho s)}{\partial \rho}. \quad (2.6)$$

These identities will be needed later, as well as the definitions of the heat capacity at constant volume c (the traditionally used subscript v omitted) and the generalised van der Waals parameter a ,

$$c = \frac{\partial e}{\partial T}, \quad a = - \frac{\partial e}{\partial \rho}. \quad (2.7)$$

For the van der Waals fluid, c and a are both constant (independent of ρ and T).

2.2. Governing equations

A flow of non-ideal fluid will be characterised by the density ρ , temperature T , and velocity $\mathbf{v} = (u, v, w)$, all depending on the spatial coordinates (x, y, z) and time t . Assume also that the fluid is affected by a bulk force \mathbf{F} , which will be later identified with the intermolecular attraction (sometimes referred to as the van der Waals attraction).

Using the identity

$$\frac{1}{\rho} \nabla p = s \nabla T + \nabla G$$

[which follows from (2.4)], one can write the standard hydrodynamic equations in the form

$$\frac{\partial \rho}{\partial t} + \nabla \cdot (\rho \mathbf{v}) = 0, \quad (2.8)$$

$$\frac{\partial \mathbf{v}}{\partial t} + (\mathbf{v} \cdot \nabla) \mathbf{v} + s \nabla T + \nabla G = \frac{1}{\rho} \nabla \cdot \boldsymbol{\Pi} + \mathbf{F}, \quad (2.9)$$

$$\rho c \left(\frac{\partial T}{\partial t} + \mathbf{v} \cdot \nabla T \right) + [\mathbf{I} (p + a \rho^2) - \boldsymbol{\Pi}] : \nabla \mathbf{v} - \nabla \cdot (\kappa \nabla T) = 0, \quad (2.10)$$

where the dotless product of two vectors produces a second-order tensor, the symbol $:$ denotes the double scalar product of such tensors, \mathbf{I} is the identity matrix,

$$\boldsymbol{\Pi} = \mu_s \left[\nabla \mathbf{v} + (\nabla \mathbf{v})^T - \frac{2}{3} \mathbf{I} (\nabla \cdot \mathbf{v}) \right] + \mu_b \mathbf{I} (\nabla \cdot \mathbf{v}) \quad (2.11)$$

is the viscous stress tensor, μ_s (μ_b) is the shear (bulk) viscosity, and κ , the thermal conductivity. Note that μ_s , μ_b , κ , c , and a depend generally on ρ and T .

The diffuse-interface model (DIM) assumes that the intermolecular attractive force is given by

$$\mathbf{F} = K \nabla \nabla^2 \rho, \quad (2.12)$$

where the Korteweg parameter K is a constant (does not depend on ρ and T).

Equations (2.8)–(2.11) (with an unspecified force \mathbf{F}) have been derived by van Beijeren & Ernst (1973) from Enskog’s theory of dense fluids, and the full set (2.8)–(2.12) was derived by Giovangigli (2020) from the Enskog–Vlasov kinetic equation. For numerous other derivations (through irreversible thermodynamics and similar models), see the references cited by Giovangigli (2020); Giovangigli & Matuszewski (2013).

2.3. Boundary conditions at the substrate

Assume that the fluid is bounded below by a solid substrate whose shape is given by $z = H(x, y)$ – see figure 2. This implies the no-flow boundary condition,

$$\mathbf{v} = \mathbf{0} \quad \text{at} \quad z = H. \quad (2.13)$$

Let the substrate be kept at a fixed temperature,

$$T = T_0 \quad \text{at} \quad z = H. \quad (2.14)$$

Due to the presence of higher-order derivatives of ρ in expression (2.9) for the intermolecular force, an extra boundary condition is required for the density. There are several versions of such in the literature (Seppecher 1996; Pismen & Pomeau 2000), of which the simplest is used in this work,

$$\rho = \rho_0 \quad \text{at} \quad z = H, \quad (2.15)$$

where ρ_0 is a phenomenological parameter. The physical meaning of this condition can be clarified by considering the van der Waals force acting on the fluid in the near-substrate boundary layer: the solid attracts it *toward* the substrate while the fluid outside the boundary layer pulls it *away* from the substrate. The former force is fixed, whereas the latter grows with the near-substrate density, so the balance is achieved when the density assumes a certain value – precisely as prescribed by condition (2.15).

In addition to the advantage of simplicity, condition (2.15) has the advantage of applicability under the same assumptions as the DIM itself (Benilov 2020*b*). Furthermore,

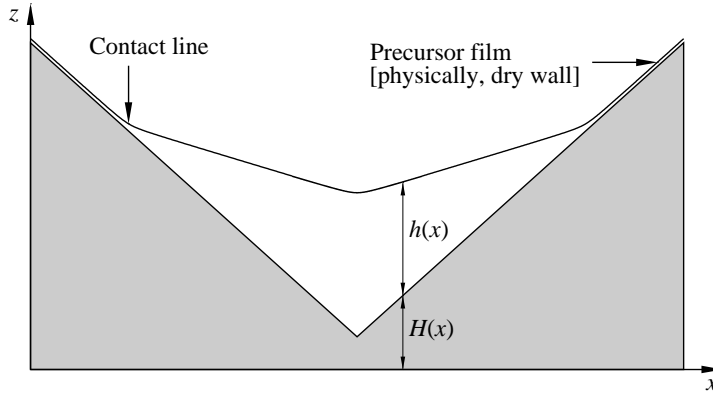


Figure 2: Formulation of the problem.

since the expected effect of spontaneous condensation depends only on the curvature of the meniscus interface (as argued in the introduction), the model used for the boundary condition is not essential. Indeed, condensation occurs at the liquid/vapour interface, so the fluid–substrate interaction does not affect it too much.

2.4. Boundary conditions far above the substrate

Assume that, far above the substrate, the tangential stress and vertical heat are both zero,

$$\frac{\partial \mathbf{v}}{\partial z} \rightarrow \mathbf{0} \quad \text{as} \quad z \rightarrow +\infty, \quad (2.16)$$

$$\frac{\partial T}{\partial z} \rightarrow 0 \quad \text{as} \quad z \rightarrow +\infty. \quad (2.17)$$

Let the variations of the density field be vertically localised, so that ρ tends to a constant – say, ρ_∞ . If ρ_∞ exceeds the density ρ_v of saturated vapour, the fluid – with or without the meniscus – is thermodynamically unstable, making the whole setting physically meaningless. If, on the other hand, $\rho_\infty < \rho_v$, the problem becomes trivial, as liquid surrounded by undersaturated vapour, obviously, evaporates. Thus, assume

$$\rho \rightarrow \rho_v \quad \text{as} \quad z \rightarrow +\infty. \quad (2.18)$$

The density ρ_v of saturated vapour, together with the matching liquid density ρ_l , depend on the temperature and are determined by the so-called Maxwell construction,

$$G(\rho_v, T) = G(\rho_l, T), \quad (2.19)$$

$$p(\rho_v, T) = p(\rho_l, T). \quad (2.20)$$

In what follows, the substrate temperature is assumed to be subcritical, in which case equations (2.19)–(2.20) admit a unique solution for the pair (ρ_v, ρ_l) such that $\rho_v < \rho_l$ and

$$\left(\frac{\partial p}{\partial \rho} \right)_{\rho=\rho_v} \geq 0, \quad \left(\frac{\partial p}{\partial \rho} \right)_{\rho=\rho_l} \geq 0.$$

These two conditions guarantee that the vapour and liquid are thermodynamically stable (the pressure grows with ρ). Note also that p in the above inequalities can be replaced with the chemical potential G , as their derivatives with respect to ρ are of the same sign [see first identity in (2.4)].

Physically, the Maxwell construction ensures that a liquid/vapour interface is stable: the equalities of the chemical potential and pressure in the two phases guarantee the thermodynamic and mechanical equilibria, respectively. Note that, typically, the fluid density varies between ρ_v and ρ_l , but never equals either of them – yet it can be infinitely close to these values in a region far away from all the interfaces. Mathematically, (2.19)–(2.20) can be derived from the DIM (or any other adequate model) by adapting the governing equations for the static isothermal flat interface in unbounded space (more details given below).

Let the near-substrate density prescribed by boundary condition (2.15) be such that

$$\rho_v < \rho_0 < \rho_l. \quad (2.21)$$

If this condition does not hold, the substrate becomes either perfectly hydrophobic (if $\rho_0 \leq \rho_v$) or perfectly hydrophilic (if $\rho_0 \geq \rho_l$) (Pismen & Pomeau 2000; Benilov 2020*b*). In the former case, condensation cannot occur on the substrate (as it repulses the liquid phase), whereas the latter implies immediate condensation regardless of all other parameters.

2.5. How can one distinguish phases in a continuous density field?

Since the DIM assumes the density to vary continuously (as opposed to be restricted to ρ_v or ρ_l), one needs a formal definition of the position of the interface between the phases. The simplest option is to assume that the fluid with $\rho > (\rho_v + \rho_l)/2$ is liquid, and vice versa.

Thus, the liquid/vapour interface is defined to be located at the height $z = h + H$, where $h(x, y, t)$ is such that

$$\rho(x, y, h + H, t) = \frac{1}{2}(\rho_v + \rho_l). \quad (2.22)$$

To ensure that $h > 0$, one should require [in addition to restriction (2.21)] that

$$\rho_0 > \frac{1}{2}(\rho_v + \rho_l). \quad (2.23)$$

Due to this condition, a layer exists adjacent to the substrate, where the fluid density is ‘squeezed’ between the left and right sides of (2.23); according to definition (2.22), this layer is to be designated as ‘liquid’. Thus, even if one considers a horizontally-localised drop or meniscus, this layer stretches to infinity in all horizontal directions (see figure 2) – which was probably what prompted Pismen & Pomeau (2000) to dub it a “precursor film”. Yet, physically, it corresponds to dry substrate.

Due the presence of an unbounded precursor film around a localised meniscus, a formal definition of a contact line is needed. To formulate it, introduce the thickness \bar{h} of the precursor film on a infinitely-large flat substrate (as shown below, \bar{h} depends on the fluid’s equation of state and the Korteweg parameter K).

Next, consider a meniscus on a non-flat substrate; in this work, its contact line will be defined as the set of points (x_{cl}, y_{cl}) – typically, a contour – where

$$h(x_{cl}, y_{cl}, t) = 2\bar{h}. \quad (2.24)$$

Outside this contour, the substrate is assumed to be covered by the precursor film.

Thus, the precursor film is, essentially, a solid/vapour interface. By comparison with sizes of capillary menisci (ranging from 0.1 mm to 10 mm), its thickness \bar{h} is miniscule.

In what follows, such scales will be referred to as *microscopic*.

3. Static menisci

3.1. Preliminaries

Let the fluid be at rest, $\mathbf{v} = \mathbf{0}$, which also implies isothermality $T = T_0$ (otherwise the heat flux would generate a flow) and steadiness of the density field, $\partial\rho/\partial t = 0$. With this in mind and considering for simplicity the *two-dimensional* (2D) case, one can reduce (2.8)–(2.12) to a single equation for $\rho(x, y)$,

$$G(\rho, T) - K \left(\frac{\partial^2 \rho}{\partial x^2} + \frac{\partial^2 \rho}{\partial z^2} \right) = G(\rho_v, T), \quad (3.1)$$

where T_0 was replaced with T and the value of the constant of integration on the right-hand side was deduced from boundary condition (2.18). Physically, this (elliptic nonlinear) equation describes the balance of the van der Waals force and pressure gradient.

To nondimensionalise equation (3.1), introduce a density scale ϱ , a characteristic value A of the van der Waals parameter, and the interfacial thickness

$$l_i = \sqrt{\frac{K}{A}}. \quad (3.2)$$

Estimates carried out by Magaletti *et al.* (2016); Gallo *et al.* (2020); Benilov (2020*b*) show that l_i is on a nanometer scale.

Everywhere in this paper, the vertical-to-horizontal aspect ratio ε of menisci are assumed to be small. Accordingly, the following nondimensional variables will be used:

$$x_{nd} = \frac{x}{\varepsilon^{-1}l_i}, \quad z_{nd} = \frac{z}{l_i}, \quad H_{nd} = \frac{H}{l_i}, \quad (3.3)$$

$$\rho_{nd} = \frac{\rho}{\varrho}, \quad T_{nd} = \frac{RT}{A\varrho}, \quad (3.4)$$

$$G_{nd} = \frac{G}{A\varrho}, \quad p_{nd} = \frac{p}{A\varrho^2}, \quad s_{nd} = \frac{s}{R}, \quad (3.5)$$

where R is the specific gas constant. Introduce also

$$(\rho_0)_{nd} = \frac{\rho_0}{\varrho}. \quad (3.6)$$

In terms of the new variables, equation (3.1) takes the form (the subscript $_{nd}$ omitted)

$$G(\rho, T) - \varepsilon^2 \frac{\partial^2 \rho}{\partial x^2} - \frac{\partial^2 \rho}{\partial z^2} = G(\rho_v, T). \quad (3.7)$$

The nondimensional versions of the boundary condition and the Maxwell construction will not be presented, as they look exactly as their dimensional counterparts (2.15), (2.18) and (2.19)–(2.20), respectively.

As shown by Pismen & Pomeau (2000); Benilov (2020*c*), the smallness of the meniscus's aspect ratio requires that the near-substrate density be close to the density of the liquid phase – i.e.,

$$\rho_0 = \rho_l - \varepsilon. \quad (3.8)$$

This equality can be viewed as the formal definition of ε through ρ_l and ρ_0 .

3.2. 1D solutions of equation (3.7)

First consider the solution $\bar{\rho}(z)$ of equation (3.7) that describes a *flat* liquid/vapour interface in an *unbounded* space (i.e., without a substrate). For this case, (3.7) and (2.18) yield

$$G(\bar{\rho}, T) - \frac{d^2\bar{\rho}}{dz^2} = G(\rho_v, T), \quad (3.9)$$

$$\bar{\rho} \rightarrow \rho_v \quad \text{as} \quad z \rightarrow +\infty, \quad (3.10)$$

which should be complemented with

$$\bar{\rho} \rightarrow \rho_l \quad \text{as} \quad z \rightarrow -\infty. \quad (3.11)$$

Due to the translational invariance of this boundary-value problem, its solution is not unique. To make it such, require

$$\bar{\rho}(0) = \frac{1}{2}(\rho_l + \rho_v). \quad (3.12)$$

For a physically meaningful $G(\rho, T)$, $\bar{\rho}(z)$ is a kink-like function, decreasing monotonically with increasing z .

The boundary-value problem for $\bar{\rho}(z)$ can be used to derive the Maxwell construction. Its first ‘half’ – equality (2.19) – can be derived by considering equation (3.9) in the limit $z \rightarrow -\infty$. Equation (2.20), in turn, can be obtained by multiplying (3.9) by $d\bar{\rho}/dz$ and integrating; taking into account identity (2.5) and fixing the constant of integration via boundary condition (3.10), one obtains

$$\bar{\rho}G(\bar{\rho}, T) - p(\bar{\rho}, T) - \frac{1}{2} \left(\frac{d\bar{\rho}}{dz} \right)^2 = \bar{\rho}G(\rho_v, T) - p(\rho_v, T). \quad (3.13)$$

Considering this equation in the limit $z \rightarrow -\infty$ and using equation (2.19) (as it has already been proved), one can obtain (2.20) as required.

Next, let there be a substrate, and let it be flat; without loss of generality, one can set in this case $H = 0$. The solution describing this situation can be obtained by shifting $\bar{\rho}(z)$ along the z axis by a distance \bar{h} such that

$$\bar{\rho}(-\bar{h}) = \rho_0.$$

Physically, the solution $\rho = \bar{\rho}(z - \bar{h})$ describes the precursor film, and \bar{h} is its nondimensional thickness. One can deduce from (separable) equation (3.13) that

$$\bar{h} = \int_{\frac{1}{2}(\rho_l + \rho_v)}^{\rho_0} \frac{2^{-1/2} d\rho}{\sqrt{\rho [G(\rho, T) - G(\rho_v, T)] - p(\rho, T) + p(\rho_v, T)}}. \quad (3.14)$$

To estimate this integral asymptotically, observe that the Maxwell construction (2.19)–(2.20) and identity (2.5) imply

$$\begin{aligned} & 2[\rho G(\rho, T) - p(\rho, T) - \rho G(\rho_v, T) + p(\rho_v, T)] \\ & = C^2(\rho - \rho_l)^2 + \mathcal{O}[(\rho - \rho_l)^3] \quad \text{as} \quad \rho \rightarrow \rho_l, \end{aligned} \quad (3.15)$$

where

$$C = \left[\left(\frac{\partial G}{\partial \rho} \right)_{\rho=\rho_l} \right]^{1/2}. \quad (3.16)$$

Assume that the liquid is thermodynamically stable (which is the only case worth considering). Hence, $(\partial G/\partial \rho)_{\rho=\rho_l} > 0$, and C is real.

Asymptotic (3.15) shows that the integrand in (3.14) has a first-order pole at $\rho = \rho_l$. This pole is located *outside* the integration interval, but not too far from its upper limit [recall that ρ_0 is close to ρ_l due to (3.8)]. One can thus derive that

$$\bar{h} = \frac{\ln \varepsilon^{-1}}{C} + \mathcal{O}(1). \quad (3.17)$$

One can also deduce from equation (3.13) and asymptotic (3.15) that

$$\frac{d\bar{\rho}(z - \bar{h})}{dz} = \mathcal{O}(\varepsilon) \quad \text{for} \quad z \leq 0. \quad (3.18)$$

Estimates (3.17)–(3.18) will be used later.

3.3. An example: the van der Waals fluid

For the van der Waals fluid, the nondimensional specific internal energy and entropy are

$$e(\rho, T) = cT - \rho, \quad s(\rho, T) = c \ln T - \rho \ln \frac{\rho}{1 - \rho},$$

where the heat capacity c has been nondimensionalised by R . The corresponding expression for the nondimensional pressure and chemical potential are

$$p(\rho, T) = \frac{T\rho}{1 - \rho} - \rho^2,$$

$$G(\rho, T) = T \left(\ln \frac{\rho}{1 - \rho} + \frac{1}{1 - \rho} + c - c \ln T \right) - 2\rho.$$

The solution of the Maxwell construction (2.19)–(2.20) for this case is shown in figure 3(a); note also that the critical temperature of the van der Waals fluid is $T_{cr} = 8/27$.

It is instructive to examine the limit $T \rightarrow 0$ which applies to many common fluids at room temperature (see Table 1 Benilov 2020a). In this limit, the asymptotic solution of the Maxwell construction is (Benilov 2020c),

$$\rho_l = \frac{1 + \sqrt{1 - 4T}}{2} + \mathcal{O}(e^{-1/T}),$$

$$\rho_v = \frac{1 + \sqrt{1 - 4T}}{1 - \sqrt{1 - 4T}} e^{-1/T} + \mathcal{O}(T^{-1} e^{-2/T}).$$

Thus, if T is small, the vapour density is *exponentially* small, and the same can be assumed for all physically meaningful equations of states, not only for the van der Waals one.

For $T \ll 1$, one can deduce from boundary-value problem (3.9)–(3.12) that

$$\bar{\rho}(z) \approx \begin{cases} 1 & \text{if } z \leq -2^{-3/2}\pi, \\ \frac{1}{2} (1 - \sin 2^{1/2}z) & \text{if } -2^{-3/2}\pi \leq z \leq 2^{-3/2}\pi, \\ 0 & \text{if } z \geq 2^{-3/2}\pi. \end{cases} \quad (3.19)$$

The accuracy of this formula is $\mathcal{O}(T \ln T)$.

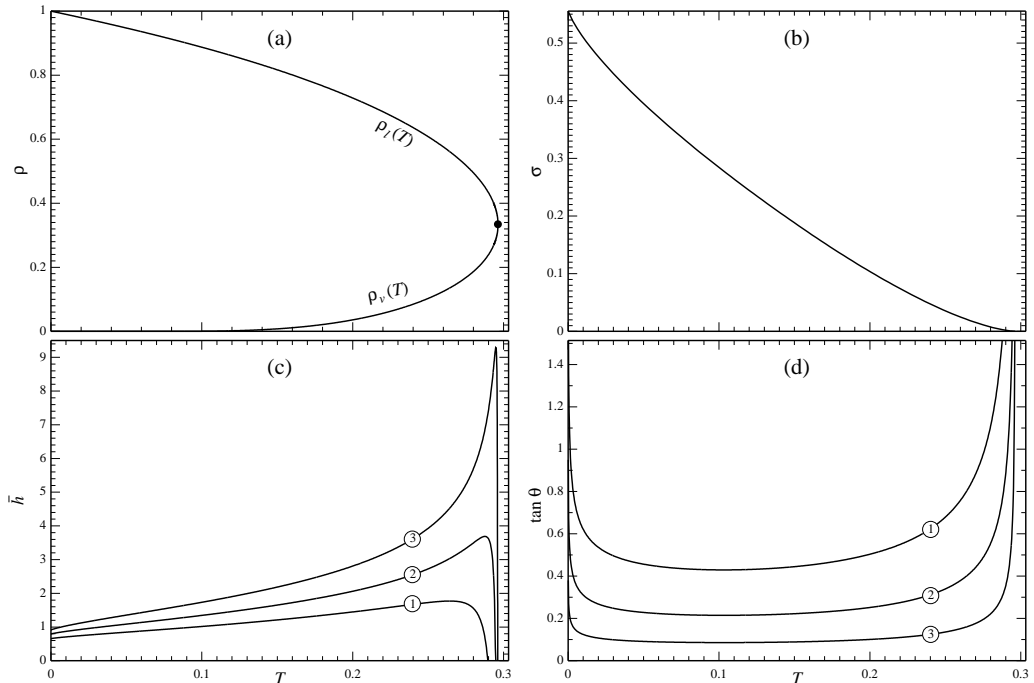


Figure 3: Various characteristics of interfaces and contact lines *vs* the temperature: (a) densities of the liquid and vapor phases (the black dot marks the critical point); (b) surface tension; (c) precursor film's thickness; (d) $\tan \theta$, where θ is the contact angle. The curves in panels (c) and (d) correspond to (1) $\varepsilon = 0.1$; (2) $\varepsilon = 0.05$; (3) $\varepsilon = 0.02$.

3.4. Asymptotic description of static menisci

Consider a static fluid configuration with the liquid phase confined to a layer adjacent to the substrate, forming a meniscus (2D liquid film). This implies that, with increasing z , the density first grows from ρ_0 to approximately ρ_l , then decreases towards ρ_v .

Everywhere in this paper, it will be assumed that the meniscus's thickness is of the order of, or greater than, the precursor film's thickness,

$$h \gtrsim \bar{h}. \quad (3.20)$$

As shown below, all static menisci satisfy this assumption, so it is not too restrictive.

The asymptotic description of menisci with a small aspect ratio is based on the observation that, to leading order, the general equation (3.7) for $\rho(x, z)$ coincides with equation (3.9) for $\bar{\rho}(z)$ – and the corresponding boundary conditions (2.18) and (3.10) coincide identically.

Having this in mind and comparing definition (2.22) of h with the ‘midpoint condition’ (3.12) for $\bar{\rho}$, one can deduce that

$$\rho(x, z) = \bar{\rho}(z - h - H) + \mathcal{O}(\varepsilon). \quad (3.21)$$

The error of this ansatz is due to the difference between the exact boundary condition (2.15) and its counterpart (3.10) for $\bar{\rho}$. Indeed, subject to assumption (3.20), ansatz (3.21)

yields $\rho(x, H) \approx \rho_l$ – which matches the corresponding exact value, ρ_0 , with an error of $\mathcal{O}(\varepsilon)$.

Using (3.21), one can derive the following asymptotic equation for $h(x)$ (for technical details, see Appendix A):

$$\sigma \frac{d^2(h + H)}{dx^2} = f(\bar{h} - h). \quad (3.22)$$

Here

$$\sigma = \int_{-\infty}^{\infty} \left(\frac{d\bar{\rho}}{dz} \right)^2 dz \quad (3.23)$$

is, physically, the surface tension of the liquid/vapour interface and

$$f(\bar{h} - h) = 2C^2 \left[1 - e^{C(\bar{h}-h)} \right] e^{C(\bar{h}-h)}, \quad (3.24)$$

where C is defined by (3.16), and \bar{h} by (3.14).

The coefficients $\sigma(T)$ and $\bar{h}(T, \varepsilon)$ have been computed for the van der Waals fluid and are shown in figures 3(b,c), respectively. The former shows that the surface tension vanishes at the critical point (as it should). Note also that, since $\rho_v \rightarrow \rho_l$ as $T \rightarrow T_{cr}$ [see figure 3(a)] – then, sooner or later, $\rho_0 = \rho_l - \varepsilon$ becomes smaller than ρ_v . This violates assumption (2.21) and also makes \bar{h} negative, so this part of figure 3(c) has been truncated.

3.5. Static meniscus in a corner between two solids

Before considering menisci in a corner, it is instructive to examine the solution of equation (3.22) for a *flat substrate* with the following boundary condition:

$$h \rightarrow \bar{h} \quad \text{as} \quad x \rightarrow +\infty. \quad (3.25)$$

Substituting $H = \text{const}$ into equation (3.22), multiplying it by dh/dz , integrating, and fixing the constant of integration via condition (3.25), one can obtain a separable equation. Its solution will be presented in a form that is best suited for physical interpretation:

$$h = \bar{h} + \frac{1}{C} \ln \left[1 + \exp \frac{C(x_0 - x) \tan \theta}{\varepsilon} \right], \quad (3.26)$$

where x_0 is an arbitrary constant and

$$\tan \theta = \left(\frac{2C}{\sigma} \right)^{1/2} \varepsilon. \quad (3.27)$$

The physical meaning of θ can be deduced from the following asymptotics of solution (3.26) at minus-infinity,

$$h \rightarrow -\frac{x}{\varepsilon} \tan \theta \quad \text{as} \quad x \rightarrow -\infty,$$

which describes a liquid/vapour interface inclined at an angle θ [the factor of ε accounts for the different scalings of x and z in nondimensionalisation (3.3)]. Thus, θ is the contact angle specific to the given fluid–substrate combination.

The dependence of θ on T , computed for the van der Waals fluid, is shown in figure 3(d). Observe that $\theta \rightarrow \infty$ in both small-temperature and near-critical limits (which can also be deduced analytically from the asymptotic behavior of C and σ as $T \rightarrow 0$ and $T \rightarrow T_{cr}$). As a result, the lubrication approximation fails in these limits, and so the results presented cannot be trusted.

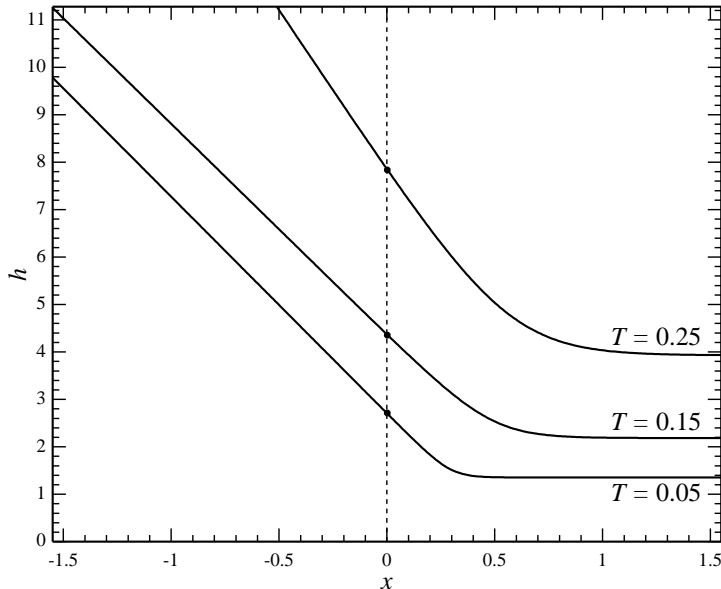


Figure 4: Examples of solution (3.20) for $\varepsilon = 0.02$ and three values of the temperature (indicated in the figure). In all three cases, the shift x_0 is chosen in such a way that the position of the contact lines [defined by condition (2.24)] is $x_{cl} = 0$ (the black dots mark the points where (2.24) holds).

Examples of solution (3.26) computed for the van der Waals fluid are shown in figure 4. Observe that the interfaces for $T = 0.05$ and $T = 0.15$ are almost parallel, which is a result of near-constancy of θ in the middle part of figure 3(d).

Next, let the substrate form a corner of angle ϕ (as in figure 2), so that the substrate is described by

$$H = |x| \varepsilon^{-1} \tan \frac{\pi - \phi}{2}. \quad (3.28)$$

Since the lubrication approximation used in this paper implies that $\theta \ll 1$ and $\phi \approx \pi$, the tan can be omitted in (3.27)–(3.28) can be omitted, but it can be just as well be kept (so that the results obtained would look physically natural).

Given the substrate's symmetry, the meniscus surface should also be symmetric, i.e.,

$$\frac{d(h + H)}{dx} = 0 \quad \text{at} \quad x = 0. \quad (3.29)$$

Assume also that, far from the corner the substrate is dry, which amounts to boundary condition (3.25).

Since, in the problem at hand,

$$\frac{d^2 H}{dx^2} = 0 \quad \text{if} \quad x \neq 0,$$

the general equation (3.22) reduces for $x > 0$ to that describing an inclined interface over

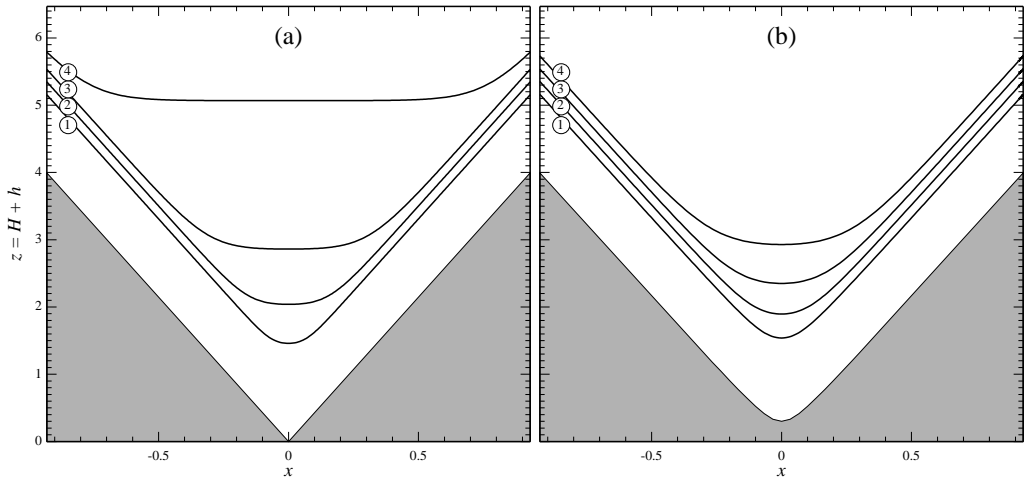


Figure 5: Examples of static menisci with $\varepsilon = 0.02$, in a corner with $\tan \frac{1}{2}(\pi - \phi) = 0.085875$. Curves (1)–(4) correspond to $T = 0.025, 0.05, 0.075, 0.1$. (a) Solution (3.30) for the sharp corner. (b) The numerical solution for the smooth corner described by expression (3.33)–(3.34).

a *flat* substrate. Using thus the same approach to finding the solution, one calculates

$$h = \bar{h} + \frac{1}{C} \ln \left[1 - \frac{\tan \frac{1}{2}(\pi - \phi)}{\tan \frac{1}{2}(\phi) - \tan \theta} \exp \left(-\frac{C|x|\tan \theta}{\varepsilon} \right) \right]. \quad (3.30)$$

Evidently, h is real for all x – hence, physically meaningful – only if

$$\frac{1}{2}(\pi - \phi) \leq \theta. \quad (3.31)$$

Not surprisingly, this condition (of existence of static menisci) is the opposite of condition (1.1) of condensation.

Another restriction on applicability of solution (3.30) originates from the requirement that h be non-negative,

$$\tan \frac{1}{2}(\pi - \phi) \geq -\left(e^{C\bar{h}} - 1\right) \tan \theta. \quad (3.32)$$

Evidently, this condition can be violated only if ϕ is reflex.

Examples of static menisci described by solution (3.30) are shown in figure 5(a). They are all computed for the angle ϕ such that the existence condition (3.31) holds everywhere except a narrow interval near

$$0.1027 \lesssim T \lesssim 0.1033.$$

Evidently, when T approaches this interval, the core (middle part) of the meniscus becomes infinitely thick. This does not violate the lubrication approximation, however, as the slope of the interface remains small.

As for condition (3.32), it can be violated – at least, for the van der Waals fluid – only if T is very near its critical value and ϕ is near 2π . These requirements cut out a minuscule part of the problem’s parameter space, not to mention that $\tan \theta$ is not small there – hence, the lubrication approximation fails. This effectively means that restriction (3.32) can be ignored.

Note, however, that substrates with a *sharp* corner – such as the one given by (3.28) – violate the lubrication approximation. One can still argue that the corner can be smoothed by an arc with a radius of curvature much larger than the thickness of the meniscus, but much smaller than the meniscus’s width. In this case, the lubrication approximation holds, and the solutions should be asymptotically close to that for the sharp corner.

It turns out, however, that smoothing of the corner changes the nature of the vapour instability, making this case worth studying. The general tendency will be illustrated by the following example of the substrate’s shape:

$$H = \sqrt{\left(x\varepsilon^{-1} \tan \frac{\pi - \phi}{2}\right)^2 + H_0^2 e^{-(x/\Delta_H)^2}}, \quad (3.33)$$

where the constants H_0 and Δ_H determine the amplitude and width of smoothing. Equation (3.22) cannot be in this case solved analytically, but its solution can be found using the MATLAB function BVP4c (based on the three-stage Lobatto IIIa formula Kierzenka & Shampine 2001). Typical results are shown in figure 5(b); comparing it with 5(a), one can see that the smoothing mostly affects *near-critical* solutions: when the temperature approaches to the threshold when they cease to exist, the menisci do not spread out like those in the sharp corner with the same ‘global’ angle ϕ .

The solution existence region in the problem’s parameters space also changes slightly. If, for example,

$$H_0 = 0.3, \quad \Delta = 1, \quad (3.34)$$

the static-meniscus solution exists if

$$\tan \frac{1}{2} (\pi - \phi) \lesssim 0.0872,$$

which marginally expands the similar condition for the sharp corner,

$$\tan \frac{1}{2} (\pi - \phi) \lesssim 0.0859.$$

(the right-hand side of the latter inequality is the approximate value of $\tan \theta$).

The difference between the two existence criteria would be too slight to be important, should it not seem to invalidate the suggested physical interpretation of the main result of this paper, condition (1.1). If condensation does not occur in a situation where it holds, does this mean that concave menisci do not absorb moisture?

To resolve the apparent paradox, observe that a sufficiently small drop can have its contact lines in the *smoothed region* and, thus, not be sensitive to the global angle ϕ – as a result, it could be static. On the other hand, a sufficiently large drop with contact lines on the *flat* parts of the walls should still be unstable.

Mathematically, existence of a static meniscus – even a stable one with respect to infinitesimal perturbation – does not necessarily mean the vapour is stable with respect to *finite-amplitude* perturbations. This issue will be clarified in the next section by solving a partial differential equation describing the evolution of fluid in a corner.

4. Evolving menisci

As shown in the previous section, steady menisci in a sharp corner exist only subject to condition (3.30), but it is still unclear what happens if (3.30) does not hold. One can only assume that menisci evolve in this case.

To find out how exactly they evolve, two evolution equations have been derived: one

applicable when $\rho_v/\rho_l \sim 1$ (Appendix B.1) and one for $\rho_v/\rho_l \ll 1$ (Appendix B.2). According to the former, the dynamics is dominated by expansion (compression) of the fluid while it evaporates (condensates) – whereas, under the latter, these effects are as strong as advection by horizontal velocity. Motion-induced variations of temperature are small in both cases, but they can be neglected only in the latter regime (in the former, they still affect the leading-order dynamics). Finally, the latter equation applies to many common fluids at room temperature Benilov (2020a) – and, thus, will be discussed in detail; the solutions of the former are qualitatively similar and, thus, will not.

The regime $\rho_v/\rho_l \ll 1$ is governed by

$$\rho_l^2 \frac{\partial h}{\partial t} + \frac{\partial}{\partial x} \left\{ Q(h) \frac{\partial}{\partial x} \left[\sigma \frac{\partial^2 (h+H)}{\partial x^2} - f(\bar{h}-h) \right] \right\} = \frac{1}{\varepsilon^2 D} \left[\sigma \frac{\partial^2 (h+H)}{\partial x^2} - f(\bar{h}-h) \right], \quad (4.1)$$

where the function f is defined by (3.24) and the rest of the coefficients are

$$D = \rho_l^2 \int_{-\infty}^{\infty} \frac{\mu_b(\bar{\rho}, T) + \frac{4}{3} \mu_s(\bar{\rho}, T)}{\bar{\rho}^4} \left(\frac{\partial \bar{\rho}}{\partial z} \right)^2 dz, \quad (4.2)$$

$$Q(h) = \int_0^{\infty} \frac{\hat{\rho}^2(z-h)}{\mu_s(\bar{\rho}(z-h), T)} dz, \quad (4.3)$$

$$\hat{\rho}(z) = \int_z^{\infty} [\bar{\rho}(z') - \rho_v] dz'. \quad (4.4)$$

To understand the physical meaning of equation (4.1), note that the two terms involving $f(\bar{h}-h)$ describe how the substrate affects the liquid/vapour interface (since h is the distance between the two, it does not come as a surprise that $f \rightarrow 0$ as $h \rightarrow \infty$). Out of the two terms involving σ , the one on the left-hand side is the usual capillary term, whereas the one on the right-hand side describes either evaporation or condensation (the Kelvin effect). Which one, depends on the curvature of the liquid/vapour interface: if it is convex (concave), this term is negative (positive) and, thus, causes evaporation (condensation). Note also that, if $H = \text{const}$, equation (4.1) coincides with its flat-substrate counterpart derived by Benilov (2020c).

Since equation (4.1) has been obtained for the case $\rho_v/\rho_l \ll 1$, this assumption can also be used to simplify the expressions for the coefficients D and Q .

Firstly, the main contribution to the integral in (4.2) comes from the region where ρ is small – comparable to ρ_v – and so the vapour there is close to ideal gas. As a result, D can be calculated using the van der Waals equation of state (which can be viewed as a generic extension of the ideal-gas equation and, thus, is quantitatively correct in the low-density region). Secondly, one can assume that the viscosities μ_s and μ_b are proportional to the density – hence, given an appropriate choice of the nondimensionalisation scale μ , one can let

$$\mu_s(\rho, T) = \rho, \quad \mu_b(\rho, T) = \mu'_b \rho,$$

where μ'_b is an order-one constant. Thirdly, an appropriate choice of the density scale allows one to set

$$\rho_l = 1. \quad (4.5)$$

Fourthly, when calculating $Q(h)$, one can use the small- T asymptotics of $\bar{\rho}(z)$ [for the van der Waals fluid, this amounts to expression (3.19)]. Note that such asymptotics is not accurate enough for small ρ and, thus, is too crude for calculating D (in particular, it rounds off ρ_v to zero – hence, the integral in (4.2) diverges).

Under these four assumptions, (4.2)–(4.4) can be reduced to (Benilov 2020*c*)

$$D \approx 0.36994 \left(\mu'_b + \frac{4}{3} \right) T^{1/2} \rho_v^{-3/2}, \quad (4.6)$$

$$\begin{aligned} Q(h) &\approx \frac{1}{3} h^3 + 2^{-1/2} \pi (1 - \ln 2) - 2^{-9/2} 3^{-1} \pi^3 \\ &\approx \frac{1}{3} h^3 + 0.22489. \end{aligned} \quad (4.7)$$

Note that expression (4.7) has been obtained specifically for the van der Waals ; for a different equation of state, the numeric constant would be different. The same assumptions can be used to obtain asymptotic expressions for C , σ , and \bar{h} , but expressions (3.14), (3.16), and (3.23) which determine these parameters are simple enough as they are.

By comparison with (second-order) equation (3.22) for static menisci, equation (4.1) requires two extra boundary conditions. One of these follows from the symmetry of the problem, implying zero exchange of fluid between the regions $x < 0$ and $x > 0$ – hence, the no-through-flow boundary condition (see Appendix B.2) should be applied,

$$\frac{\partial}{\partial x} \left[\sigma \frac{\partial^2 (h + H)}{\partial x^2} - f(\bar{h} - h) \right] = 0 \quad \text{at} \quad x = 0. \quad (4.8)$$

The second additional boundary condition is simply

$$\frac{\partial h}{\partial x} \rightarrow 0 \quad \text{as} \quad x \rightarrow +\infty. \quad (4.9)$$

Equation (4.1) with its coefficients determined by (3.14), (3.16), (3.23), and (4.6)–(4.7), and boundary conditions (3.25), (3.29), (4.8)–(4.9) have been solved numerically using the method of lines (Schiesser 1978) for numerous initial conditions, in a wide range of the parameters involved. The results of the simulations indicated that, in all cases where the condensation criterion (1.1) was satisfied, a meniscus was growing as $t \rightarrow \infty$.

A typical evolution is shown in figure 6(a), computed for zero bulk viscosity,

$$\mu'_b = 0 \quad (4.10)$$

and

$$T = 0.1, \quad \varepsilon = 0.02, \quad (4.11)$$

in which case the contact angle is $\tan \theta \approx 0.0859$. The corner was such that

$$\tan \frac{1}{2} (\pi - \phi) = 0.1, \quad (4.12)$$

so that the vapour is weakly unstable. The initial condition was

$$h + H = \sqrt{\left(x \varepsilon^{-1} \tan \frac{\pi - \phi}{2} \right)^2 + h_0 e^{-(x/\Delta_h)^2}} \quad \text{at} \quad t = 0, \quad (4.13)$$

with

$$h_0 = 1, \quad \Delta_h = 1 \quad (4.14)$$

[(4.13) looks similar to expression (3.33) for H , but they are not be confused).

The following features of figure 6 should be observed:

- Initially, a quick adjustment occurs [observe the large difference between curves (1) and (2)].
- At large times, the growth of the meniscus slows down, at a rate which seems to be logarithmic – i.e., fairly small.

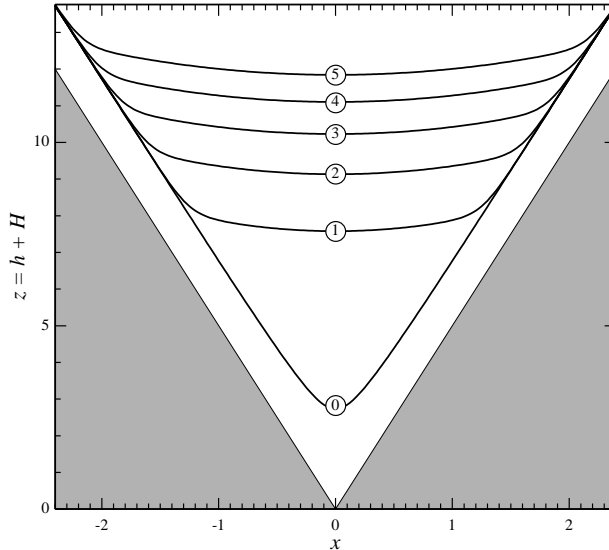


Figure 6: An example of a growing meniscus, for parameters (4.10)–(4.14). The curve number n and the time are related by the formula $t = 40n$.

Another feature is quantified in figure 7 showing the thickness of the meniscus and the slope of the interface *vs* x for $t = 200$ (which corresponds to curve 5 in figure 6):

- For large times, the ‘core’ of the meniscus assumes the spherical-cap shape (under the lubrication approximation, this corresponds to a parabolic dependence of h on x). Indeed, observe that, in the core, the interfacial slope changes *linearly* from 0 (horizontal interface) to

$$\frac{\partial(h+H)}{\partial x} = \varepsilon^{-1} \left[\tan \frac{1}{2}(\pi - \phi) - \tan \theta \right] \quad (4.15)$$

(i.e., the angle between the interface and substrate equals θ). As seen in figure 7(b), $\partial(h+H)/\partial x$ assumes value (4.15) on the boundary separating the core and the near-contact-line zone; in the latter, the interface becomes parallel to the substrate, i.e.,

$$\lim_{x \rightarrow \infty} \frac{\partial(h+H)}{\partial x} = \varepsilon^{-1} \tan \frac{1}{2}(\pi - \phi) \quad (4.16)$$

(for the parameters corresponding to figure 7, the right-hand side of equation (4.16) is equal to 5). Finally, figure 7(a) shows that the meniscus thickness in the near-contact-line zone is close to that of the precursor film.

Figure 8 shows typical evolution of a meniscus in a smoothed corner, computed for $H(x)$ given by (3.33)–(3.34) with

$$\tan \frac{\pi - \phi}{2} = 0.0871 \quad (4.17)$$

the fluid parameters given by (4.11), and the initial condition given by (4.13) with

$$h_0 = 2, \quad \Delta_h = 0.5. \quad (4.18)$$

Even though a steady solution exists in this case, the meniscus grows as $t \rightarrow \infty$. It

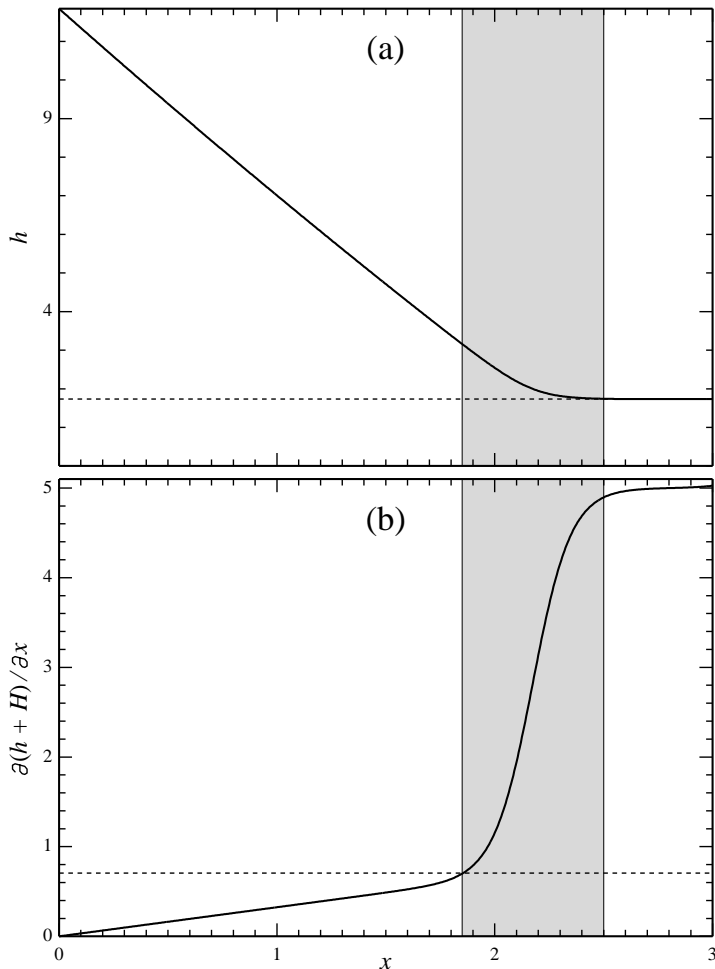


Figure 7: The cross-section of the growing meniscus with parameters (4.10)–(4.11), for $t = 200$ (corresponds to curve 5 in Fig. 6): (a) thickness of the meniscus, $h(x)$; (b) slope of the interface, $\partial(h + H)/\partial x$. The near-contact-line zone is shaded. The dotted line in panel (b) corresponds to the slope given by (4.15).

would not grow, and become static, only if the amplitude of the initial perturbation is sufficiently small – for the initial condition (4.13) with $\Delta_h = 0.5$, this occurs if $h_0 \lesssim 1.851$.

Extensive numerical experiments with various initial conditions showed that, to make the meniscus grow, its initial volume has to be sufficiently high, whereas its shape is unimportant: if it is too ‘narrow’ or too ‘wide’, it quickly spreads out or contracts (the nondimensional timescale of this stage is 10^{-2}). The end result of the adjustment is a meniscus with its surface being as flat as possible, and the further evolution depends on how wide the (adjusted) meniscus is. For growth, it should cover an area comparable to the smoothed part of the corner – otherwise it tends to the existing steady state and becomes static.

Most importantly, the adjusted meniscus does not have to be thick to initiate growth, and its nondimensional thickness is order-one. In dimensional terms, this means that the

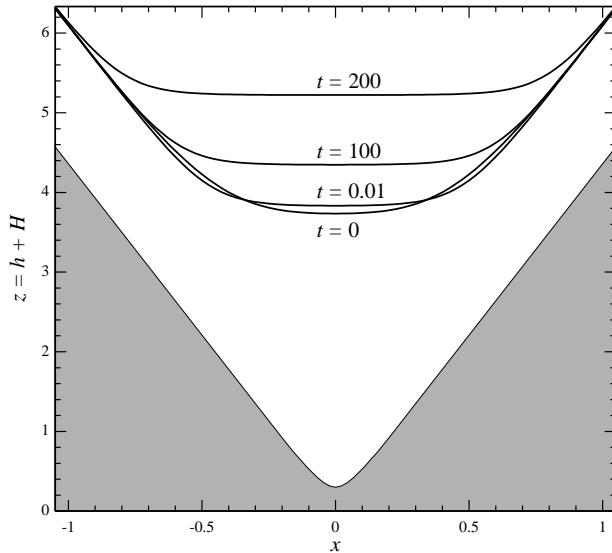


Figure 8: An example of a growing meniscus in a smooth corner, for parameters (3.33)–(3.34), (4.10)–(4.13), (4.17)–(4.18). The times corresponding to the curves are shown in the figure (observe that they are not equally spaced).

instability is triggered off by *microscopic* perturbations, i.e., those representing a liquid film whose thickness is comparable to the interfacial thickness.

5. Why has spontaneous condensation yet to be observed?

Recall that the coordinates and meniscus thickness h are nondimensionalised by the interfacial thickness l_i which is much smaller than the scale L of macroscopic capillary phenomena, such as drops and menisci. Thus, spontaneous condensation is definitely observable only at a microfluidic scale, whereas its relevance to macroscopic phenomena needs to be verified by estimating its characteristic time scale.

To clarify this issue, one should rewrite equation (4.1) in terms of dimensional variables and balance the time derivative with the term responsible for condensation (as discussed in the previous section, this is the first term on the right-hand side). The resulting timescale of spontaneous condensation is

$$t_{sc} = \frac{T^{1/2}}{\rho_v^{3/2}} \frac{\mu L^2}{\eta l_i}, \quad (5.1)$$

where μ (introduced initially for nondimensionalisation) should be identified with the shear viscosity at the given temperature, and

$$\eta = \varrho^2 (AK)^{1/2} \sigma \quad (5.2)$$

is, physically, the dimensional surface tension. Formula (5.2), however, can only be used if one knows the Korteweg constant K and the fluid's equation of state (to compute σ), making it much more practical to measure the surface tension η directly or take from a handbook.

As for l_i [which also appears in expression (5.1)], one can use numerous indirect estimates (Magaletti *et al.* 2016; Gallo *et al.* 2020; Benilov 2020*b*, e.g.) suggesting that

$$l_i = 10^{-9} \text{ m.}$$

The nondimensional parameter ρ_v , in turn, should be identified with the air to water density ratio. Estimating it at, say, 25°C, one obtains

$$\rho_v \approx 1.2 \times 10^{-3}.$$

For the nondimensional temperature (if the dimensional one is 25°C), the estimate of Benilov (2020*a*) will be used,

$$T = 0.14.$$

Then, letting the scale L of macroscopic capillary phenomena be 1 mm, one can use (5.1) to obtain

$$t_{sc} \approx 31.5 \text{ h,}$$

which can be viewed as a characteristic timescale of spontaneous condensation of fully saturated humid air at room temperature.

The above estimate explains why spontaneous condensation has not been observed before: simply because no-one thought that watching saturated air for more than a day would make for interesting viewing.

Now, with the theory of this effect in place, one can observe it on a much quicker scale. To do so, one should carry out an experiment at a temperature comparable, but necessarily close, to the critical temperature. As a result, the vapour-to-liquid density ration would not be small, making the effect of spontaneous condensation much quicker.

Overall, measuring the parameters of spontaneous condensation should be as easy as measuring those of evaporating drops – and the latter *have* been measured on numerous occasions (e.g. Birdi *et al.* 1989; Birdi & Vu 1993; Rowan *et al.* 1995).

6. Concluding remarks

The main tool used in the present paper – equation (4.1) – can also be used for modeling thin sessile drops with contact lines. To make it convenient to use, it will be rewritten in terms of the dimensional variables and in the form not involving the specifics of the fluid’s equation of state. The former can be eliminated by

- (i) evaluating the coefficient D for the van der Waals fluid;
- (ii) simplifying D under the assumption $T \ll 1$ [applicable to many common fluids at room temperature (Benilov 2020*a*)]; and
- (iii) replacing the numeric coefficients with undetermined constants (to be fixed as the best fit to experimental data, as always done when modeling contact lines).

Apart from D , equation (4.1) also involves ε (the relative difference between the near-substrate fluid density and that of the liquid phase). This parameter cannot be measured directly, but it can be eliminated through equation (3.27) relating ε to the (measurable) contact angle θ . As for the interfacial scale l_i and precursor film thickness \bar{h} , they will be – in the spirit of item (iii) above – left undetermined†.

† Alternatively, one can use the (presumably known) thermodynamic properties of the fluid to calculate the nondimensional surface tension σ and substitute it – together with the measured dimensional surface tension η – into expression (5.2). This way, (5.2) can be used to determine K , after which l_i can be calculated through Eq. (3.2). As for \bar{h} , it can be deduced from the fluid’s thermodynamic properties using (3.14).

With all this in place, equation (4.1) takes the form

$$\begin{aligned} \frac{\mu}{\eta} \frac{\partial h}{\partial t} + \nabla \cdot \left\{ \left(\frac{1}{3} h^3 + b_1 l_i^3 \right) \nabla \left[\nabla^2 (h + H) - \frac{\tan \theta}{\tau^{1/2} l_i} f \left(\frac{\bar{h} - h}{\tau^{1/2} l_i} \right) \right] \right\} \\ = \frac{b_2 l_i}{\tau^{1/2}} \left(\frac{\rho_a}{\rho_l} \right)^{3/2} \left[\nabla^2 (h + H) - \frac{\tan \theta}{\tau^{1/2} l_i} f \left(\frac{\bar{h} - h}{\tau^{1/2} l_i} \right) \right], \end{aligned} \quad (6.1)$$

where b_1 and b_2 are undetermined order-one constants, the variables h , t , x , and y are now dimensional, μ is the shear viscosity, η is the surface tension, ρ_a and ρ_l are the dimensional densities of air and liquid, respectively, and

$$f(\xi) = (1 - e^\xi) e^\xi. \quad (6.2)$$

The nondimensional temperature (denoted now by τ , with T being the *dimensional* temperature) is

$$\tau = \frac{RT}{A\rho_l},$$

where R is the specific gas constant and the van der Waals parameter A can be related to the critical pressure p_c and critical temperature T_c via the formula (Haynes *et al.* 2017)

$$A = \frac{27R^2 T_c^2}{64p_c}.$$

To understand, in what way (6.1) differs for the existing liquid-film models incorporating the Kelvin effect (e.g. Deegan *et al.* 2000; Eggers & Pismen 2010; Colinet & Rednikov 2011; Rednikov & Colinet 2013; Morris 2014; Janeček *et al.* 2015; Stauber *et al.* 2015; Saxton *et al.* 2016; Brabcova *et al.* 2017; Rednikov & Colinet 2019; Wray *et al.* 2019), note that there are two distinct mechanisms of evaporation of drops:

- (a) through *diffusion* of vapour in the surrounding air, and
- (b) through *advection* of vapour by the flow due to the variations of the chemical potential (caused by the curvature of the drop's surface).

All of the existing models are based on mechanism (a), whereas the present work, on mechanism (b). The latter is concerned with *pure* fluids, where diffusion does not occur (recall that equation (2.8) does not include a diffusion term). In *multicomponent* fluids, however, both mechanism should be accounted for – but, so far, only (a) has.

Declaration of interests

The authors report no conflict of interests.

Appendix A. Derivation of equation (3.22)

Multiply equation (3.7) by $\partial\rho/\partial z$ and use identity (2.5) to rearrange the result in the form

$$\frac{\partial}{\partial z} \left[\frac{1}{2} \left(\frac{\partial\rho}{\partial z} \right)^2 \right] = \frac{\partial}{\partial z} [\rho G(\rho, T) - p(\rho, T) - \rho G(\rho_v, T)] - \varepsilon^2 \frac{\partial\rho}{\partial z} \frac{\partial^2\rho}{\partial x^2}.$$

Integrate this equation and fix the constant of integration (which is actually a function of x) via boundary condition (2.18), which yields

$$\frac{1}{2} \left(\frac{\partial\rho}{\partial z} \right)^2 = \rho G(\rho, T) - p(\rho, T) - \rho G(\rho_v, T) + p(\rho_v, T) + \varepsilon^2 \left[\int_H^z F(x, z') dz' - f \right], \quad (A1)$$

where

$$f = \int_H^\infty F(x, z) dz, \quad F(x, z) = -\frac{\partial \rho(x, z)}{\partial z} \frac{\partial^2 \rho(x, z)}{\partial x^2}.$$

Substituting ansatz (3.21) into the expression for f and taking into account boundary condition (3.10), one obtains

$$f = -\frac{1}{2} \left\{ \frac{d(h+H)}{dx} \left[\frac{d\bar{\rho}(z-h-H)}{dz} \right]_{z=H} \right\}^2 + \frac{d^2(h+H)}{dx^2} \int_H^\infty \left[\frac{d\bar{\rho}(z-h-H)}{dz} \right]^2 dz. \quad (\text{A } 2)$$

This expression can be simplified using estimate (3.18): it allows one to discard the first term on the right-hand side and extend the integral in the second term from H to $-\infty$ (neither results in leading-order error). Thus, to leading order,

$$f = \frac{d^2(h+H)}{dx^2} \sigma, \quad (\text{A } 3)$$

where σ is given by (3.23).

To make (A 3) into a closed-form equation for $h(x)$, it remains to relate f to h – which can be done using the exact equation (A 1). One does not need its full solution to find h : as follows from the definition (2.22) of h , one only needs the part between the substrate and the midpoint of the interface.

This effectively means that the first (integral) term in the square brackets on the right-hand side of equation (A 1) can be omitted.

Indeed, since this integrand in this term involves $d\bar{\rho}/dz$, it is small everywhere except near the interface. f , on the other hand, is order-one everywhere between the interface and substrate – which is an asymptotically wider region due to estimate (3.17). Thus, any characteristic of the solution in the latter region can be calculated with the integral term in equation (A 1) omitted.

After that, (A 1) turns into a separable ordinary differential equation. It admits two types of solutions:

(T1) those that decay monotonically from the $\rho(0) = \rho_0$ to $\rho(\infty) = \rho_v$, and

(T2) those that grow until they reach a maximum – say, $\rho = \rho_m$ – and then start to decay [examples of such solutions are shown in figure 1 of (Benilov 2020c)].

Depending on the type of solution, h is represented by

$$\text{T1:} \quad h = - \int_{\rho_0}^{\frac{1}{2}(\rho_l + \rho_v)} \frac{d\rho}{\sqrt{2[\rho G(\rho, 1) - p(\rho, 1) - \rho G(\rho_v, 1) + p(\rho_v, 1) - \varepsilon^2 f]}}, \quad (\text{A } 4)$$

$$\text{T2:} \quad h = \int_{\rho_0}^{\rho_m} \frac{d\rho}{\sqrt{2[\rho G(\rho, 1) - p(\rho, 1) - \rho G(\rho_v, 1) + p(\rho_v, 1) - \varepsilon^2 f]}} - \int_{\rho_m}^{\frac{1}{2}(\rho_l + \rho_v)} \frac{d\rho}{\sqrt{2[\rho G(\rho, 1) - p(\rho, 1) - \rho G(\rho_v, 1) + p(\rho_v, 1) - \varepsilon^2 f]}}, \quad (\text{A } 5)$$

where ρ_m satisfies the equation

$$\rho_m G(\rho_m, 1) - p(\rho_m, 1) - \rho_m G(\rho_v, 1) + p(\rho_v, 1) - \varepsilon^2 f = 0. \quad (\text{A } 6)$$

Case T1 of monotonic solutions will be examined first. As follows from expression (3.8) for ρ_0 and expansion (3.15), the neighborhood of the lower limit contributes significantly to the integral. This does not mean, however, that the contribution of the rest of the interval

can be ignored. To take into account both contributions, the integrand of (A 4) will be represented by the sum of its ‘inner’ and ‘outer’ approximations minus the matching part (the same way as the composite solution is constructed in the method of matched asymptotics). The inner approximation can be obtained by expanding the expression under the square root about $\rho = \rho_l$ – the outer approximation, by omitting the small term $\varepsilon^2 f$ – and the matching part, by either omitting $\varepsilon^2 f$ in the former or expanding the latter. Taking into account expression (3.8) and expansion (3.15), one obtains

$$h = \int_{\frac{1}{2}(\rho_l + \rho_v)}^{\rho_l - \varepsilon} \left[\frac{1}{\sqrt{C^2 (\rho - \rho_l)^2 - 2\varepsilon^2 f}} + \frac{1}{\sqrt{2[\rho G(\rho, 1) - p(\rho, 1) - \rho G(\rho_v, 1) + p(\rho_v, 1)]}} - \frac{1}{G'_v(\rho_l - \rho)} \right] d\rho, \quad (\text{A } 7)$$

where C is given by (3.13). The first and third integrals in (A 7) can be evaluated explicitly, and the second can be identified with \bar{h} given by expression (3.14); as result, one obtains

$$h = \frac{1}{C} \ln \frac{2C}{C + \sqrt{C^2 - 2f}} + \bar{h},$$

This equality should be viewed as an equation for f ; solving it, one obtains (3.24) as required [and equation (A 3) coincides with equation (3.22)].

Case T2 of non-monotonic solutions will not be discussed in detail. It will only be mentioned that the asymptotic solution of equation (A 6) is

$$\rho_m = \rho_l - \frac{(2f)^{1/2}}{C} \varepsilon + \mathcal{O}(\varepsilon^2).$$

Since both ρ_0 and ρ_m are close to ρ_l , the first integral in (A 5) can be estimated by expanding the integrand about $\rho = \rho_l$, whereas the second integral should be treated in the same manner as that in (A 4). In the end, this case yields exactly the same dependence of f on h as (3.24).

Appendix B. Asymptotic equations for evolving menisci

For simplicity, the asymptotic analysis in this appendix will be carried out for the two-dimensional (2D) case. The 3D versions of the equations derived can be easily deduced afterwards from the requirement of horizontal isotropy.

As mentioned in the main body of the paper, there are two asymptotic regimes in this problem, depending on the parameter ρ_v/ρ_l . The common part of their asymptotic analyses will be presented first, with the regime-specific parts to follow.

To nondimensionalise the governing equations, assume that the shear and bulk viscosities are of the same order, $\mu_s \sim \mu_b$, and introduce a scale μ representing them both. As shown by Benilov (2020c) for a flat substrate, the scale for the horizontal velocity u should be deduced from the balance of the viscous and Korteweg stress, resulting in

$$V = \frac{\varepsilon^3 A \varrho^2 l_i}{\mu}, \quad (\text{B } 1)$$

where A , ϱ , and l_i have been defined in the beginning of §3. The scale for the vertical velocity w is regime-specific and will be chosen later – as is, and will be, the time scale. Assume also that the heat capacity is comparable to the specific gas constant R .

In addition to the nondimensional variables defined by (3.3)–(3.6), introduce

$$u_{nd} = \frac{u}{V}, \quad (\text{B2})$$

$$c_{nd} = \frac{c}{R}, \quad a_{nd} = \frac{a}{A}, \quad (\text{B3})$$

$$(\mu_s)_{nd} = \frac{\mu_s}{\mu}, \quad (\mu_b)_{nd} = \frac{\mu_b}{\mu}, \quad \kappa_{nd} = \frac{\kappa}{\varkappa}, \quad (\text{B4})$$

where \varkappa is a characteristic scale of the thermal conductivity.

B.1. Asymptotic limit $\rho_v/\rho_l \sim 1$

Let the nondimensional time and vertical velocity be

$$t_{nd} = \frac{t}{l_i/(\varepsilon^{-1}V)}, \quad w_{nd} = \frac{w}{\varepsilon^{-1}V}. \quad (\text{B5})$$

Substituting (3.3)–(3.6) and (B2)–(B5) into the 2D version of boundary-value problem (2.8)–(2.18) and omitting the subscript nd , one obtains

$$\frac{\partial \rho}{\partial t} + \boxed{\varepsilon^2} \frac{\partial(\rho u)}{\partial x} + \frac{\partial(\rho w)}{\partial z} = 0, \quad (\text{B6})$$

$$\begin{aligned} & \boxed{\alpha \varepsilon^2} \left(\frac{\partial u}{\partial t} + \boxed{\varepsilon^2} u \frac{\partial u}{\partial x} + w \frac{\partial u}{\partial z} \right) + \boxed{\frac{1}{\varepsilon^2}} \left[s \frac{\partial T}{\partial x} + \frac{\partial}{\partial x} \left(G - \boxed{\varepsilon^2} \frac{\partial^2 \rho}{\partial x^2} + \frac{\partial^2 \rho}{\partial z^2} \right) \right] \\ & = \frac{1}{\rho} \left\{ \frac{\partial}{\partial x} \left[2 \boxed{\varepsilon^2} \mu_s \frac{\partial u}{\partial x} + \left(\mu_b - \frac{2}{3} \mu_s \right) \left(\boxed{\varepsilon^2} \frac{\partial u}{\partial x} + \frac{\partial w}{\partial z} \right) \right] + \frac{\partial}{\partial z} \left[\mu_s \left(\frac{\partial u}{\partial z} + \frac{\partial w}{\partial x} \right) \right] \right\}, \end{aligned} \quad (\text{B7})$$

$$\begin{aligned} & \boxed{\alpha \varepsilon^2} \left(\frac{\partial w}{\partial t} + \boxed{\varepsilon^2} u \frac{\partial w}{\partial x} + w \frac{\partial w}{\partial z} \right) + \boxed{\frac{1}{\varepsilon^2}} \left[s \frac{\partial T}{\partial z} + \frac{\partial}{\partial z} \left(G - \boxed{\varepsilon^2} \frac{\partial^2 \rho}{\partial x^2} + \frac{\partial^2 \rho}{\partial z^2} \right) \right] \\ & = \frac{1}{\rho} \left\{ \boxed{\varepsilon^2} \frac{\partial}{\partial x} \left[\mu_s \left(\frac{\partial u}{\partial z} + \frac{\partial w}{\partial x} \right) \right] + \frac{\partial}{\partial z} \left[2 \mu_s \frac{\partial w}{\partial z} + \left(\mu_b - \frac{2}{3} \mu_s \right) \left(\boxed{\varepsilon^2} \frac{\partial u}{\partial x} + \frac{\partial w}{\partial z} \right) \right] \right\}, \end{aligned} \quad (\text{B8})$$

$$\begin{aligned} & \boxed{\alpha \gamma} \rho c \left(\frac{\partial T}{\partial t} + \boxed{\varepsilon^2} u \frac{\partial T}{\partial x} + w \frac{\partial T}{\partial z} \right) + \boxed{\beta} (p + a \rho^2) \left(\boxed{\varepsilon^2} \frac{\partial u}{\partial x} + \frac{\partial w}{\partial z} \right) \\ & = \boxed{\beta \varepsilon^2} \left\{ \mu_s \left[2 \boxed{\varepsilon^4} \left(\frac{\partial u}{\partial x} \right)^2 + \boxed{\varepsilon^2} \left(\frac{\partial u}{\partial z} + \frac{\partial w}{\partial x} \right)^2 + 2 \left(\frac{\partial w}{\partial z} \right)^2 \right] \right. \\ & \quad \left. + \left(\mu_b - \frac{2}{3} \mu_s \right) \left(\boxed{\varepsilon^2} \frac{\partial u}{\partial x} + \frac{\partial w}{\partial z} \right)^2 \right\} + \frac{\partial}{\partial x} \left(\kappa \frac{\partial T}{\partial x} \right) + \boxed{\frac{1}{\varepsilon^2}} \frac{\partial}{\partial z} \left(\kappa \frac{\partial T}{\partial z} \right), \end{aligned} \quad (\text{B9})$$

$$u = 0, \quad w = 0 \quad \text{at} \quad z = H, \quad (\text{B10})$$

$$\frac{\partial u}{\partial z} \rightarrow 0, \quad \frac{\partial w}{\partial z} \rightarrow 0 \quad \text{as} \quad z \rightarrow \infty, \quad (\text{B11})$$

$$\rho = \rho_0, \quad T = T_0 \quad \text{at} \quad z = H, \quad (\text{B12})$$

$$\rho \rightarrow \rho_v, \quad \frac{\partial T}{\partial z} \rightarrow 0 \quad \text{as} \quad z \rightarrow \infty, \quad (\text{B } 13)$$

where

$$\alpha = \frac{K\varrho^3}{\mu^2}, \quad \beta = \frac{A\varrho^4 K}{\mu\kappa(T_0)_d},$$

$$\gamma = \frac{C\mu}{\kappa}, \quad T_0 = \frac{R(T_0)_d}{A\varrho},$$

and $(T_0)_d$ is the dimensional temperature of the substrate.

The positions where α appears in equations (B 7)–(B 8) suggest that it represents the Reynolds number, β is the ‘‘isothermality parameter’’ introduced by Benilov (2020*a*), and γ is the Prandtl number.

In each of equations (B 7)–(B 9), there are terms proportional to $1/\varepsilon^2$ – which can cancel only if

$$T = T_0 + \varepsilon^2 \tilde{T}, \quad (\text{B } 14)$$

$$G(\rho, T) - \varepsilon^2 \frac{\partial^2 \rho}{\partial x^2} - \frac{\partial^2 \rho}{\partial z^2} = G(\rho_v, T_0) + \varepsilon^2 \tilde{G}, \quad (\text{B } 15)$$

where ρ_v is calculated at $T = T_0$. According to (B 14), the temperature variations are small – which does not mean, however, that their effect on the film dynamics is negligible. To make it such, one should also assume the isothermality parameter β to be small (Benilov 2020*c*).

Upon substitution of (B 14)–(B 15) into boundary-value problem (B 6)–(B 13), one can see that, to leading-order, equation (B 7) and the boundary conditions for u decouple from the other equations and boundary conditions. The former are thus omitted, and the latter take the form

$$\frac{\partial \rho}{\partial t} + \frac{\partial(\rho w)}{\partial z} = \mathcal{O}(\varepsilon^2), \quad (\text{B } 16)$$

$$s \frac{\partial \tilde{T}}{\partial z} + \frac{\partial \tilde{G}}{\partial z} - \frac{1}{\rho} \frac{\partial}{\partial z} \left(\eta \frac{\partial w}{\partial z} \right) = \mathcal{O}(\varepsilon^2), \quad (\text{B } 17)$$

$$-\beta (p + a\rho^2) \frac{\partial w}{\partial z} + \frac{\partial}{\partial z} \left(\kappa \frac{\partial \tilde{T}}{\partial z} \right) = \mathcal{O}(\varepsilon^2), \quad (\text{B } 18)$$

$$w = 0, \quad \tilde{T} = 0 \quad \text{at} \quad z = H, \quad (\text{B } 19)$$

$$\frac{\partial w}{\partial z} \rightarrow 0, \quad \frac{\partial \tilde{T}}{\partial z} \rightarrow 0 \quad \text{as} \quad z \rightarrow \infty, \quad (\text{B } 20)$$

$$\rho = \rho_0 \quad \text{at} \quad z = H, \quad (\text{B } 21)$$

$$\rho \rightarrow \rho_v \quad \text{as} \quad z \rightarrow \infty, \quad (\text{B } 22)$$

where the ‘effective viscosity’ λ is given by

$$\lambda = \mu_b + \frac{4}{3}\mu_s, \quad (\text{B } 23)$$

and s , p , a , μ_s , and μ_b are all evaluated at $T = T_0$.

Equation (B 15) can too be rewritten with the thermodynamic functions evaluated at $T = T_0$,

$$\frac{\partial^2 \rho}{\partial z^2} = G(\rho, T_0) - G(\rho_v, T_0) + \varepsilon^2 \left[\frac{\partial G(\rho, T_0)}{\partial T_0} \tilde{T} - \tilde{G} - \frac{\partial^2 \rho}{\partial x^2} \right] + \mathcal{O}(\varepsilon^4), \quad (\text{B } 24)$$

which implies the following boundary condition

$$\lim_{z \rightarrow \infty} \tilde{G} = \frac{\partial G(\rho_v, T_0)}{\partial T_0} \lim_{z \rightarrow \infty} \tilde{T} + \mathcal{O}(\varepsilon^2). \quad (\text{B } 25)$$

The asymptotic theory for evolving menisci can be developed as a natural extension of that for static ones. Firstly, ansatz (3.21) remains intact, with the only correction $h(x) \rightarrow h(x, t)$. Secondly, equation (B 24) can be rearranged into form (A 1) albeit with a different expression for F .

The simplest way to derive this expression consists in multiplying equation (B 24) by $\partial \rho / \partial z$ and adding the result to equation (B 17) multiplied by $\varepsilon^2 (\rho - \rho_0)$. Straightforward algebra involving the use of identity (2.5) yields

$$\frac{\partial}{\partial z} \left[\frac{1}{2} \left(\frac{\partial \rho}{\partial z} \right)^2 \right] = \frac{\partial}{\partial z} [\rho G - p - \rho G(\rho_v, T_0)] + \varepsilon^2 F + \mathcal{O}(\varepsilon^4), \quad (\text{B } 26)$$

where

$$F = \frac{\partial \rho}{\partial z} \left(\frac{\partial G}{\partial T} \tilde{T} - \tilde{G} - \frac{\partial^2 \rho}{\partial x^2} \right) - (\rho - \rho_0) \left[s \frac{\partial \tilde{T}}{\partial z} + \frac{\partial \tilde{G}}{\partial z} - \frac{1}{\rho} \frac{\partial}{\partial z} \left(\lambda \frac{\partial w}{\partial z} \right) \right], \quad (\text{B } 27)$$

and G and s are evaluated at $T = T_0$. Introducing, as before,

$$f = \int_H^\infty F \, dz,$$

using identity (2.6), and recalling boundary conditions (B 20) and (B 25), one obtains

$$f = -T_0 \rho_0 \left[s + \left(1 - \frac{\rho}{\rho_0} \right) \rho \frac{\partial s}{\partial \rho} \right]_{\rho=\rho_v} \lim_{z \rightarrow \infty} \tilde{T} + T_0 \rho_0 \int_H^\infty s \frac{\partial \tilde{T}}{\partial z} \, dz - \int_H^\infty \frac{\rho_0 \lambda}{\rho^2} \frac{\partial \rho}{\partial z} \frac{\partial w}{\partial z} \, dz - \int_H^\infty \frac{\partial \rho}{\partial z} \frac{\partial^2 \rho}{\partial x^2} \, dz. \quad (\text{B } 28)$$

This expression – unlike its static counterpart (A 2) – involves \tilde{T} and w , which need to be expressed through ρ .

To do so, substitute ansatz (3.30) into equation (B 16), integrate it with boundary conditions (B 19) and, to leading order, obtain

$$w = \frac{\partial h}{\partial t} \frac{\bar{\rho} - \rho_0}{\bar{\rho}}. \quad (\text{B } 29)$$

where $\bar{\rho}$ is implied to depend on $z - h - H$, not just on z . Substituting (B 29) into equation (B 18), taking into account identity (2.7), and recalling (B 14), one obtains (non-leading-order terms omitted)

$$\beta T_0 \rho_0 \frac{\partial h}{\partial t} \left(\frac{\partial s}{\partial \rho} \right)_{\rho=\bar{\rho}} \frac{\partial \bar{\rho}}{\partial z} + \frac{\partial}{\partial z} \left(\kappa \frac{\partial \tilde{T}}{\partial z} \right) = 0.$$

It follows from this equation and boundary conditions (B 19)–(B 20) that, to leading

order,

$$\tilde{T} = -\beta T_0 \rho_0 \frac{\partial h}{\partial t} \int_H^z \frac{s(\bar{\rho}', T_0) - s(\rho_v, T_0)}{\kappa(\bar{\rho}', T_0)} dz',$$

where $\bar{\rho}' = \bar{\rho}(z' - h - H)$. Substitution of this expression and (B 29) into (B 28) yields

$$f \approx \sigma \frac{\partial^2 (h + H)}{\partial x^2} - (\beta B + D) \frac{\partial h}{\partial t}, \quad (\text{B 30})$$

where

$$B = T_0^2 \rho_0^2 \int_H^\infty \left\{ s(\bar{\rho}, T_0) - \left[s(\rho, T_0) + \left(1 - \frac{\rho}{\rho_0} \right) \rho \frac{\partial s(\rho, T_0)}{\partial \rho} \right]_{\rho=\rho_v} \right\} \times \frac{s(\bar{\rho}, T_0) - s(\rho_v, T_0)}{\kappa(\bar{\rho}, T_0)} dz, \quad (\text{B 31})$$

$$D = \rho_0^2 \int_H^\infty \frac{\lambda(\bar{\rho}, T_0)}{\bar{\rho}^4} \left(\frac{\partial \bar{\rho}}{\partial z} \right)^2 dz, \quad (\text{B 32})$$

$$\sigma = \int_H^\infty \left(\frac{\partial \bar{\rho}}{\partial z} \right)^2 dz. \quad (\text{B 33})$$

As explained in Appendix A, the lower limit of integration in (B 32)–(B 33) can be moved to $-\infty$; one can also replace ρ_0 with ρ_l [as justified by (3.8)]. With all this done, σ coincides with (3.23) and D , with (4.2).

The integrand in (B 31), in turn, tends to a constant as $z \rightarrow -\infty$, so the lower limit of this integral cannot be moved to $-\infty$. It can still be simplified by integrating it by parts and *then* moving the lower limit to $-\infty$. Eventually, with ρ_0 replaced with ρ_l , (B 31) becomes

$$B = B_1 h - B_2,$$

where

$$B_1 = T_0^2 \rho_l^2 \left\{ s(\rho_l, T_0) - \left[s(\rho, T_0) + \left(1 - \frac{\rho}{\rho_0} \right) \rho \frac{\partial s(\rho, T_0)}{\partial \rho} \right]_{\rho=\rho_v} \right\} \frac{s(\rho_l, T_0) - s(\rho_v, T_0)}{\kappa(\rho_l, T_0)},$$

$$B_2 = T_0^2 \rho_l^2 \int_H^\infty z \frac{\partial}{\partial z} \left\{ s(\bar{\rho}, T_0) - \left[s(\rho, T_0) + \left(1 - \frac{\rho}{\rho_0} \right) \rho \frac{\partial s(\rho, T_0)}{\partial \rho} \right]_{\rho=\rho_v} \right\} \times \frac{s(\bar{\rho}, T_0) - s(\rho_v, T_0)}{\kappa(\bar{\rho}, T_0)} dz.$$

Finally, using expression (3.24) for f (it was derived for static menisci, but is valid generally), one can reduce (B 30) to

$$[\beta (B_1 + B_2 h) + D] \frac{\partial h}{\partial t} - \sigma \frac{\partial^2 (h + H)}{\partial x^2} = 2C^2 \left[1 - e^{-C(h-\bar{h})} \right] e^{-C(h-\bar{h})}. \quad (\text{B 34})$$

This is the desired asymptotic equation describing menisci with order-one vapour-to-liquid density ratio.

B.2. Asymptotic limit $\rho_v/\rho_l \ll 1$

If ρ_v is small – then, according to expression (B 29), the vertical velocity w in the vapour phase is large. This makes sense physically: a large density difference between

vapour and liquid accelerates the flow due evaporation from the surface of the latter. Mathematically though, this circumstance makes the scaling inconsistent, and correcting this inconsistency is not easy: even though w is uniformly large everywhere in the vapour phase, its gradient (hence, the viscous stress) rapidly decays with height. As a result, there are three regions to be examined separately:

- above* the boundary of the vapour phase (where $\rho \approx \rho_v$ and $|\partial\rho/\partial z| \ll 1$),
- near* the boundary ($\rho \sim \rho_v$, $\partial\rho/\partial z \sim 1$),
- and *below* it ($\rho \sim 1$, $\partial\rho/\partial z \sim 1$).

Another difficulty stems from the fact that ρ_v/ρ_l is small only if the nondimensional temperature T_0 is small too (see §3.3). The presence of two extra small parameters (in addition to ε and $1/h$) makes the problem even more convoluted.

A way to circumvent these difficulties was proposed by Benilov (2020c) for the case of flat substrates. Fortunately, it works for the present problem as well.

It turns out that, in the asymptotic limit at hand, the timescale is larger than that in previous subsection by a factor of ε^{-2} . This implies that the vertical velocity (which is generally driven by the vertical motion of the interface) should be scaled down by the same factor. As a result, the viscous stress associated with w appears to become negligible. Yet, Benilov (2020c) argued that it should be retained in the *vertical* momentum equation due to the fact that the contribution of w to the vertical stress near the interface is actually large and affects the global dynamics.

This plan is realised below.

Let the nondimensional time and vertical velocity be

$$t_{nd} = \frac{t}{l_i/(\varepsilon V)}, \quad w_{nd} = \frac{w}{\varepsilon V}, \quad (\text{B } 35)$$

where V is given by (B 1). Ansatz (B 15) will be reused in exactly the same form as before, whereas (B 14) becomes

$$T = T_0 + \varepsilon^4 \tilde{T}, \quad (\text{B } 36)$$

with the implication that the temperature variations are too small to affect the leading-order dynamics. As a result, (B 15) yields

$$G(\rho, T) - \frac{\partial^2 \rho}{\partial z^2} - G(\rho_v, T) = \varepsilon^2 \left(\frac{\partial^2 \rho}{\partial x^2} + \tilde{G} \right) + \mathcal{O}(\varepsilon^4),$$

where T_0 has been replaced with T . As in the previous subsection, this equality can be rewritten in form (B 26); then using ansatz (3.21), one obtains

$$\sigma \frac{\partial^2 (h + H)}{\partial x^2} + \int_H^\infty \frac{\partial \rho}{\partial z} \tilde{G} \, dz = f(h - \bar{h}), \quad (\text{B } 37)$$

with σ given by (3.23) and f , by (3.24).

Substituting (B 2)–(B 7), (B 35), (B 15), and (B 36) into the 2D version of boundary-value problem (2.8)–(2.18), omitting the subscript $_{nd}$, and keeping only the ‘important’ terms, one obtains

$$\frac{\partial \rho}{\partial t} + \frac{\partial (\rho u)}{\partial x} + \frac{\partial (\rho w)}{\partial z} = 0, \quad (\text{B } 38)$$

$$\frac{\partial \tilde{G}}{\partial x} = \frac{1}{\rho} \frac{\partial}{\partial z} \left(\mu_s \frac{\partial u}{\partial z} \right), \quad (\text{B } 39)$$

$$\frac{\partial \tilde{G}}{\partial z} = \frac{\varepsilon^2}{\rho} \frac{\partial}{\partial z} \left(\lambda \frac{\partial w}{\partial z} \right), \quad (\text{B } 40)$$

$$u = 0, \quad w = 0 \quad \text{at} \quad z = H, \quad (\text{B } 41)$$

$$\frac{\partial u}{\partial z} \rightarrow 0, \quad \frac{\partial w}{\partial z} \rightarrow 0 \quad \text{as} \quad z \rightarrow \infty, \quad (\text{B } 42)$$

$$\rho = \rho_0 \quad \text{at} \quad z = H, \quad (\text{B } 43)$$

$$\rho \rightarrow \rho_v \quad \text{as} \quad z \rightarrow \infty, \quad (\text{B } 44)$$

$$\tilde{G} \rightarrow 0 \quad \text{as} \quad z \rightarrow \infty, \quad (\text{B } 45)$$

where the effective viscosity λ is given by (B 23). The equation and boundary conditions for T have been omitted (as they have decoupled from those retained).

Treating (B 39) as an equation for u and using boundary conditions (B 41)–(B 42), one obtains

$$u = - \int_H^z \frac{1}{\mu_s(\rho(x, z'', t), T)} \int_{z''}^{\infty} \frac{\partial \tilde{G}(x, z', t)}{\partial x} \rho(x, z', t) dz' dz''. \quad (\text{B } 46)$$

Substituting this expression into Eq. (B 38), recall ansatz (3.21) and boundary conditions (B 41)–(B 42), and, omitting non-leading-order terms, obtain

$$w = \left(1 - \frac{\rho_0}{\bar{\rho}} \right) \frac{\partial h}{\partial t} + \frac{1}{\bar{\rho}} \frac{\partial}{\partial x} \int_H^z \bar{\rho}(z''' - h - H) \int_H^{z'''} \frac{1}{\mu_s(\bar{\rho}'', T)} \int_{z'''}^{\infty} \frac{\partial \tilde{G}(x, z', t)}{\partial x} \bar{\rho}' dz' dz'' dz''', \quad (\text{B } 47)$$

where the functions $\bar{\rho}$, $\bar{\rho}'$, etc. depend on $(z - h - H)$, $(z' - h - H)$, etc.

Let $Z_v(x, t)$ be the boundary of the vapour phase, defined by

$$\rho(x, y, Z_v, t) = 2\rho_v,$$

where “2” can be replaced with any order-one number exceeding unity.

Observe that the right-hand side of equation (B 40) is small (proportional to ε^2) everywhere except near the level $z = Z_v$ – hence, \tilde{G} satisfies the following asymptotic ansatz:

$$\tilde{G} \approx \tilde{G}_1(x, t) \text{H}(Z_v - z), \quad (\text{B } 48)$$

where H is the Heaviside step function. Ansatz (B 48) (and the smallness of ρ_v) imply, for example, that

$$\int_{z''}^{\infty} \frac{\partial \tilde{G}(x, z', t)}{\partial x} \bar{\rho}' dz' \approx \tilde{G}_1(x, t) \hat{\rho}(z) \quad \text{if} \quad z < Z_v,$$

where $\hat{\rho}(z)$ is defined by (4.4).

In what follows, one needs $\partial w / \partial z$, not w – hence, differentiating expression (B 47) and rearranging it in terms of \tilde{G}_1 and $\bar{\rho}$, one obtains (non-leading-order terms omitted)

$$\frac{\partial w}{\partial z} = \frac{1}{\bar{\rho}^2} \frac{\partial \bar{\rho}}{\partial z} \left[\rho_0 \frac{\partial h}{\partial t} - \frac{\partial}{\partial x} \left(\frac{\partial \tilde{G}_1}{\partial x} Q \right) \right] \quad \text{if} \quad z \sim Z_v, \quad (\text{B } 49)$$

where Q is given by (4.3). Note that expression (B 49) is accurate only near the boundary of the vapour fraction, but this is sufficient as $\partial w/\partial z$ is small everywhere else.

Integrating equation (B 40), taking into account boundary condition (B 45), integrating the right-hand side of the resulting equation by parts, substituting (B 49), and using ansatz (B 48) for \tilde{G} , one obtains

$$-\tilde{G}_1 = \varepsilon^2 D \left[\rho_0 \frac{\partial h}{\partial t} - \frac{\partial}{\partial x} \left(Q \frac{\partial \tilde{G}_1}{\partial x} \right) \right], \quad (\text{B } 50)$$

where D is given by (4.2). Finally, substitution of ansatz (B 48) into equation (B 37), yields

$$\tilde{G}_1 \rho_0 \approx -\sigma \frac{\partial^2 (h + H)}{\partial x^2} + f(h - \bar{h}). \quad (\text{B } 51)$$

Using this expression to eliminate \tilde{G}_1 from (B 50) and changing $\rho_0 \rightarrow \rho_l$, one obtains equation (4.1) as required.

Finally, substitute (B 48) and (B 51) into expression (B 46) and simplifying asymptotically the result, one obtains

$$u = \int_H^z \frac{\hat{\rho}'}{\mu_s(\hat{\rho}', T)} dz' \frac{\partial}{\partial x} \left[\sigma \frac{\partial^2 (h + H)}{\partial x^2} - f(h - \bar{h}) \right],$$

where $\hat{\rho}'$ and $\bar{\rho}'$, again, depend on $z' - h - H$. It follows from this expression that the no-through-flow boundary condition is that given by (4.8).

REFERENCES

- ANDERSON, D. M., MCFADDEN, G. B. & WHEELER, A. A. 1998 Diffuse-interface methods in fluid mechanics. *Annu. Rev. Fluid Mech.* **30**, 139–165.
- VAN BELJEREN, H. & ERNST, M. H. 1973 The modified Enskog equation. *Physica* **68** (3), 437–456.
- BENILOV, E. S. 2020a Asymptotic reductions of the diffuse-interface model, with applications to contact lines in fluids. *Phys. Rev. Fluids* **5**, 084003.
- BENILOV, E. S. 2020b The dependence of the surface tension and contact angle on the temperature, as described by the diffuse-interface model. *Phys. Rev. E* **101**, 042803.
- BENILOV, E. S. 2020c Dynamics of liquid films, as described by the diffuse-interface model. *Phys. Fluids* **32**, 112103.
- BENILOV, E. S. 2020d Nonexistence of two-dimensional sessile drops in the diffuse-interface model. *Phys. Rev. E* **102**, 022802.
- BENILOV, E. S. 2021 Spontaneous condensation of saturated vapor in a corner between two solids. *arXiv.org* <https://arxiv.org/abs/2106.14224>.
- BIRDI, K. S. & VU, D. T. 1993 Wettability and the evaporation rates of fluids from solid surfaces. *J. Adhes. Sci. Technol.* **7**, 485–493.
- BIRDI, K. S., VU, D. T. & WINTER, A. 1989 A study of the evaporation rates of small water drops placed on a solid surface. *J. Phys. Chem.* **93**, 3702–3703.
- BORCIA, R. & BESTEHORN, M. 2014 Phase field modeling of nonequilibrium patterns on the surface of a liquid film under lateral oscillations at the substrate. *Int. J. Bifurcation Chaos* **24**, 1450110.
- BORCIA, R., BORCIA, I. D., BESTEHORN, M., VARLAMOVA, O., HOFNER, K. & REIF, J. 2019 Drop behavior influenced by the correlation length on noisy surfaces. *Langmuir* **35**, 928–934.
- BRABCOVA, Z., MCHALE, G., WELLS, G. G., BROWN, C. V. & NEWTON, M. I. 2017 Electric field induced reversible spreading of droplets into films on lubricant impregnated surfaces. *Appl. Phys. Lett.* **110**, 121603.
- CAHN, J. W. 1961 On spinodal decomposition. *Acta Metall.* **9**, 795–801.

- COLINET, P. & REDNIKOV, A. 2011 On integrable singularities and apparent contact angles within a classical paradigm. *Eur. Phys. J. Special Topics* **197**, 89–113.
- DEEGAN, R. D., BAKAJIN, O., DUPONT, T. F., HUBER, G., NAGEL, S. R. & WITTEN, T. A. 2000 Contact line deposits in an evaporating drop. *Phys. Rev. E* **62**, 756–765.
- DING, H. & SPELT, P. D. M. 2007 Wetting condition in diffuse interface simulations of contact line motion. *Phys. Rev. E* **75**, 046708.
- EGGERS, J. & PISMEN, L. M. 2010 Nonlocal description of evaporating drops. *Phys. Fluids* **22**, 112101.
- GALLO, M., MAGALETTI, F. & CASCIOLA, C. M. 2018 Thermally activated vapor bubble nucleation: The landau-lifshitz–van der waals approach. *Phys. Rev. Fluids* **3**, 053604.
- GALLO, M., MAGALETTI, F., COCCO, D. & CASCIOLA, C. M. 2020 Nucleation and growth dynamics of vapour bubbles. *J. Fluid Mech.* **883**, A14.
- GINZBURG, V. L. 1960 Some remarks on phase transitions of the second kind and the microscopic theory of ferroelectric materials. *Sov. Phys. Solid State* **2**, 1824–1834.
- GIOVANGIGLI, V. 2020 Kinetic derivation of diffuse-interface fluid models. *Phys. Rev. E* **102**, 012110.
- GIOVANGIGLI, V. & MATUSZEWSKI, L. 2013 Mathematical modeling of supercritical multicomponent reactive fluids. *Math. Models Methods Appl. Sci.* **23**, 2193–2251.
- HAYNES, W. M., LIDE, D. R. & BRUNO, T. J. 2017 *CRC handbook of chemistry and physics*. Boca Raton: Taylor & Francis.
- JANEČEK, V., DOUMENC, F., GUERRIER, B. & NIKOLAYEV, V. S. 2015 Can hydrodynamic contact line paradox be solved by evaporation–condensation? *J. Colloid Interface Sci.* **460**, 329–338.
- KIERZENKA, J. & SHAMPINE, L. F. 2001 A BVP solver based on residual control and the MATLAB PSE. *ACM Trans. Math. Softw.* **27**, 299–316.
- KORTEWEG, D. J. 1901 Sur la forme que prennent les équations du mouvement des fluides si l'on tient compte des forces capillaires causées par des variations de densité considérables mais continues et sur la théorie de la capillarité dans l'hypothèse d'une variation continue de la densité. *Arch. Néerl. Sci. Ex. Nat. Ser. 2* **6**, 1–24.
- MADRUGA, S. & THIELE, U. 2009 Decomposition driven interface evolution for layers of binary mixtures. II. Influence of convective transport on linear stability. *Phys. Fluids* **21**, 062104.
- MAGALETTI, F., GALLO, M., MARINO, L. & CASCIOLA, C. M. 2016 Shock-induced collapse of a vapor nanobubble near solid boundaries. *Int. J. Multiphase Flow* **84**, 34–45.
- MAGALETTI, F., MARINO, L. & CASCIOLA, C. M. 2015 Shock wave formation in the collapse of a vapor nanobubble. *Phys. Rev. Lett.* **114**, 064501.
- MORRIS, S. J. S. 2014 On the contact region of a diffusion-limited evaporating drop: a local analysis. *J. Fluid Mech.* **739**, 308–337.
- PISMEN, L. M. & POMEAU, Y. 2000 Disjoining potential and spreading of thin liquid layers in the diffuse-interface model coupled to hydrodynamics. *Phys. Rev. E* **62**, 2480–2492.
- REDNIKOV, A. & COLINET, P. 2013 Singularity-free description of moving contact lines for volatile liquids. *Phys. Rev. E* **87**, 010401.
- REDNIKOV, A. YE. & COLINET, P. 2017 Asymptotic analysis of the contact-line microregion for a perfectly wetting volatile liquid in a pure-vapor atmosphere. *Phys. Rev. Fluids* **2**, 124006.
- REDNIKOV, A. Y. & COLINET, P. 2019 Contact-line singularities resolved exclusively by the Kelvin effect: volatile liquids in air. *J. Fluid Mech.* **858**, 881–916.
- ROWAN, S. M., NEWTON, M. I. & MCHALE, G. 1995 Evaporation of microdroplets and the wetting of solid surfaces. *J. Phys. Chem.* **99**, 13268–13271.
- SAXTON, M. A., WHITELEY, J. P., VELLA, D. & OLIVER, J. M. 2016 On thin evaporating drops: When is the d^2 -law valid? *J. Fluid Mech.* **792**, 134–167.
- SCHIESSER, W. E. 1978 *The numerical method of lines: Integration of partial differential equations*. Oxford: Clarendon Press.
- SEPPECHER, P. 1996 Moving contact lines in the Cahn-Hilliard theory. *Int. J. Eng. Sci.* **34**, 977–992.
- SIBLEY, D. N., NOLD, A., SAVVA, N. & KALLIADASIS, S. 2013a The contact line behaviour of solid-liquid-gas diffuse-interface models. *Phys. Fluids* **25**, 092111.

- SIBLEY, D. N., NOLD, A., SAVVA, N. & KALLIADASIS, S. 2013*b* On the moving contact line singularity: Asymptotics of a diffuse-interface model. *Eur. Phys. J. E* **36**, 26.
- SIBLEY, D. N., NOLD, A., SAVVA, N. & KALLIADASIS, S. 2014 A comparison of slip, disjoining pressure, and interface formation models for contact line motion through asymptotic analysis of thin two-dimensional droplet spreading. *J. Eng. Math.* **94**, 19–41.
- STAUBER, J. M., WILSON, S. K., DUFFY, B. R. & SEFIANE, K. 2015 On the lifetimes of evaporating droplets with related initial and receding contact angles. *Phys. Fluids* **27**, 122101.
- THIELE, U., MADRUGA, S. & FRASTIA, L. 2007 Decomposition driven interface evolution for layers of binary mixtures. I. Model derivation and stratified base states. *Phys. Fluids* **19**, 122106.
- WRAY, A. W., DUFFY, B. R. & WILSON, S. K. 2019 Competitive evaporation of multiple sessile droplets. *J. Fluid Mech.* **884**.
- YUE, P. & FENG, J. J. 2011 Can diffuse-interface models quantitatively describe moving contact lines? *Eur. Phys. J. Spec. Top.* **197**, 37–46.
- YUE, P., ZHOU, C. & FENG, J. J. 2010 Sharp-interface limit of the Cahn–Hilliard model for moving contact lines. *J. Fluid Mech.* **645**, 279–294.